Performance analysis of a sky-wave over-the-horizon radar simulation tool

Journal:	*IEEE Transactions on Aerospace and Electronic Systems*
Manuscript ID	TAES-2023-1786
Manuscript Type:	Regular Paper
Date Submitted by the Author:	04-Dec-2023
Complete List of Authors:	Saavedra, Zenon; Universidad Nacional de Tucuman Facultad de Ciencias Exactas y Tecnologia, electronic Electricity and Computing; Consejo Nacional de Investigaciones Cientificas y Tecnicas Llanes, Adrian; Universidad Nacional de Tucuman Facultad de Ciencias Exactas y Tecnologia, electronic Electricity and Computing Alderete Hero, Gonzalo; Universidad Nacional de Tucuman Facultad de Ciencias Exactas y Tecnologia, Electronic Electricity and Computing Di Venanzio, Julian; Fuerza Aerea Argentina Elias, Ana; Universidad Nacional de Tucuman Facultad de Ciencias Exactas y Tecnologia, electronic Electricity and Computing; Consejo Nacional de Investigaciones Cientificas y Tecnicas
Keywords:	Radar signal processing, Radar signal analysis, Radar position measurement, Radar data processing, Radar detection

SCHOLARONE™
Manuscripts

Performance Analysis of a Sky-Wave Over-the-Horizon Radar Simulation Tools

ZENON SAAVEDRA
Facultad de Ciencias Exactas y Tecnología, Universidad Nacional de Tucumán, Tucumán, Argentina
Consejo Nacional de Investigaciones Científicas y Técnicas, Tucumán, Argentina

ADRIAN LLANES
Facultad de Ciencias Exactas y Tecnología, Universidad Nacional de Tucumán, Tucumán, Argentina

GONZALO ALDERETE HERO
Facultad de Ciencias Exactas y Tecnología, Universidad Nacional de Tucumán, Tucumán, Argentina

JULIAN DI VENANZIO
Dirección Nacional de Investigación y Desarrollo, Fuerza Aérea Argentina, Buenos Aires, Argentina

ANA GEORGINA ELIAS
Facultad de Ciencias Exactas y Tecnología, Universidad Nacional de Tucumán, Tucumán, Argentina
Consejo Nacional de Investigaciones Científicas y Técnicas, Tucumán, Argentina.

***Abstract*— This paper presents the main features of a skywave over-the-horizon radar simulation software and its ability to represent and detect different search scenarios. Through a series of simulations of the primary phenomena involved in the search process, the software can estimate the behaviour of a radar system in various scenarios. This capability allows the simulator to assist in selecting the most suitable radar configuration to achieve an acceptable level of successful detection probability for a given set of scenarios. It also facilitates various studies and analyses of different factors present in the behaviour of these types of radars.**

***Index Terms*— OTH Radar, Radar Simulator, Radar System, Signal Processing Radar**

I. INTRODUCTION

Skywave Over-The-Horizon (OTH) radars are specialized radar systems capable of detecting targets beyond the line of sight by leveraging the Earth's ionosphere as a reflector for the radar's emitted electromagnetic waves [1], as is schematically shown in Fig. 1.

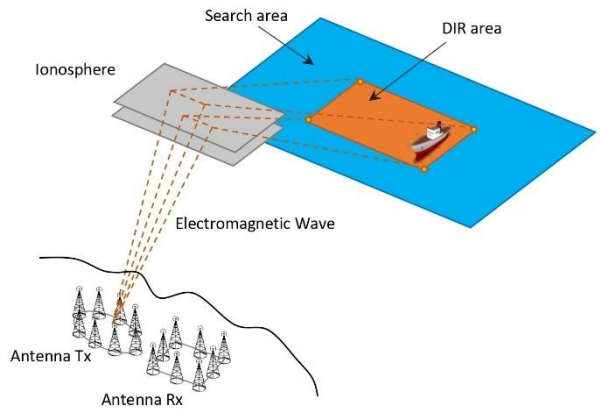

Fig. 1. OTH-SW Radar operates by reflecting its beam from the ionosphere.

The complexity and ionosphere usage of these radars imply a high manufacturing cost and a large number of components, making their preliminary study and design crucial steps before development and deployment. Computer-aided simulations serve as an effective methodology for this purpose, enabling designers to define specific radar system configurations and evaluate their performance against various proposed search scenarios. This process would ultimately determine the viability of the chosen configuration.

Several studies have presented partial models of an OTH simulator, including those by Feng et al. (2022) [2], Sun et al. (2022) [3], Cervera et al. (2018) [4] and Zhu et al. (2014) [5]. These works focus on different aspects of the OTH radar system, such as target tracking, wave propagation, interaction with the

Manuscript received XXXXX 00, 0000; revised XXXXX 00, 0000; accepted XXXXX 00, 0000. This work was supported by the Argentinian Ministry of Defence (PIDDEF program) under Grant 03/2020 and by a Post Doctoral scholarship from CONICET (Argentina) (Corresponding Z. Saavedra.)
Z. Saavedra, A. Llanes, G. Alderete Hero and A. G. Elias are with Universidad Nacional de Tucumán, Tucumán, CO 4000, Argentina, (e-mail: zsaavedra@herrera.unt.edu.ar; allanes@herrera.unt.edu.ar; herogonzalo@gmail.com; aelias@herrera.unt.edu.ar).
J. Di Venazio is with Fuerza Aerea Argentina, Buenos Aires, CO 1000, Argentina, (e-mail: jdvfaa1@gmail.com).

https://mc.manuscriptcentral.com/taes

environment and target, and sea state characterization. However, they leave out other vital aspects for system evaluation, such as signal generation, digital processing, coordinate conversion, and antenna arrays.

In this paper, we propose a comprehensive simulation software that encompasses all these phenomena, providing a more holistic representation for a thorough evaluation and analysis of system performance. Our tool encapsulates the entire search process chain, from the emission of the electromagnetic wave to the visualization of the detections. The software is intended to be included in a process to iteratively adjust the configuration setup, evaluating the alignment of detections with the proposed scenario (see Fig. 2). This leads to more accurate and complete assessment of the system's viability.

This approach gives control to the user to choose which set of parameters to keep constant and which to change. For example, the user can choose to keep the constructive parameters of the radar unchanged and optimize exploration setup for different scenarios. As another example, the user can choose specific scenarios to detect, and optimize for radar and exploration parameters. If output detections poorly match the proposed ones over different exploration setups, then radar configuration is considered inviable. Otherwise, radar config is considered viable after having acceptable detections over a large enough pool of proposed scenarios.

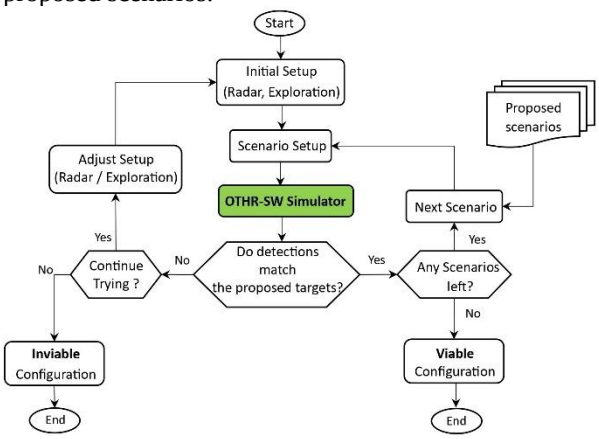

Fig. 2. Evaluation process of a radar configuration against a search scenario.

The rest of paper is organized as follows: in Section 2 we are describing the theoretical models adopted for the OTHR-SW Simulator. The results of simulations and their analyses are presented in Section 3. Conclusions are drawn in Section 4, followed by an appendix which gives further details of the simulator's configurable parameters.

II. METHODOLOGY

The OTH-SW simulator simulates the signal interaction with (i) the medium as it propagates from the transmitting array to the searching area, (ii) the searching area composed of targets and sea, as proposed by the user and (iii) the medium as the reflected energy propagates from the searching area to the receiving array.

After generating the received signal in digital domain, a digital processing module performs the "operative" stage of the radar. Here, a series of filters are applied that progressively de-noise the signal for range, doppler frequency and amplitude estimation. At the final stage, these parameters are converted to geographical coordinates and velocity, respectively. All the simulations process is represented in a block diagram in Fig. 3.

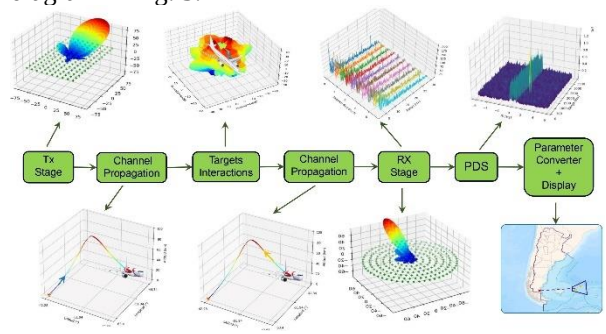

Fig. 3. General block diagram of the Skywave Over-the-Horizon (OTH-SW) Radar Simulation software.

To achieve this, we propose the following implementation scheme (also shown in Fig. 4):

- User Interface: is responsible for the interaction between the user and the simulator tool. It allows the user to input configuration parameters and visualize the output results.
- Core Entrypoint: establishes the communication channel between the front end and the core, synchronizing and controlling the data flow between blocks.
- Core: is the calculation engine of the tool that simulates the signal propagation and the radar operation to recover that signal (see Fig. 3).

https://mc.manuscriptcentral.com/taes

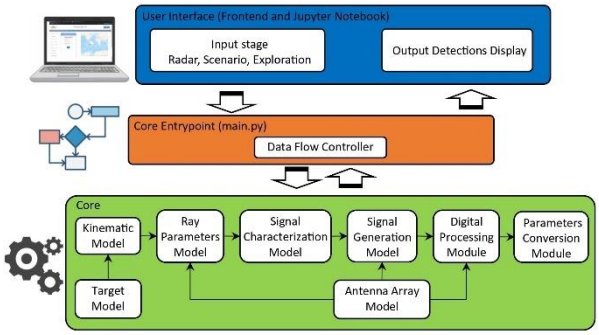

Fig. 4. Implementation scheme of (OTH-SW) Radar Simulation software.

The major blocks in the Fig. 4 are describe below with put focus in the Core implementation.

A. Input stage (Frontend)

The first step of the process is to setup all input configuration parameters exposed to the user. We classified them into a two-tier hierarchy: the top-most level has three groups:

(i) radar setup: constructive parameters of the radar.
(ii) proposed scenario setup: searching area location and targets setup.
(iii) exploration setup: parameters for shaping the exploration signal characteristics.

Each group has subgroups as shown in Fig. 5. A more thorough description can be found in the Appendix.

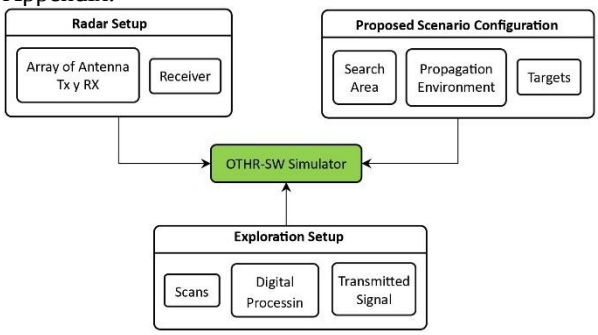

Fig. 5. Possible configuration parameters of the Over-the-Horizon Radar Simulator (OTHR-SW). The parameters are sorted into three groups: radar setup, proposed scenario, and exploration setup.

B. Target Model

The user can set up the targets for the proposed scenario. These are loaded from pre-generated files that contain target the Radar Cross Section (RCS) data.

For this work, RCS data for the following targets has been generated (shown in Fig. 6):

- Boeing 787 Aircraft
- F-117 Aircraft
- Panamax-like Vessel
- Fishing Vessel

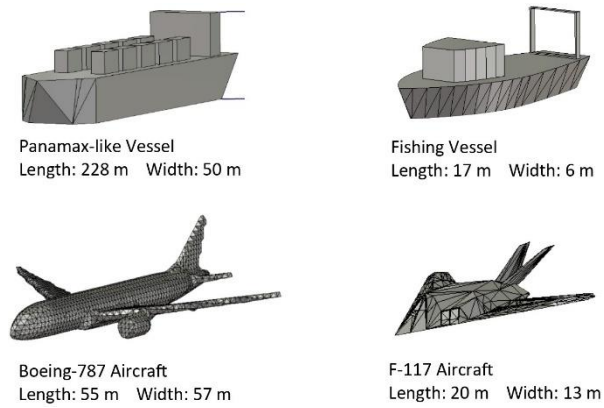

Fig. 6. Types of targets selectable in the Over-the-Horizon Radar Simulator (OTHR-SW).

1) Radar Cross Section

The radar cross section is the ability of an object to reflect a certain percentage of the electromagnetic waves that impact it. Various sources define this factor as a measure of what "an electromagnetic wave can observe on its propagation path through space". The RCS of a given target depends on aspects such as the physical structure of the target and its external characteristics, the direction of ray incidence, the frequency of the radar transmitter as well as the construction materials of the illuminated object.

In the simulator, the RCS of each target was obtained through an electromagnetic simulator software. The RCS data is stored in matrices as a function of the incident angle, carrier frequency, and wave polarization. Fig. 7 presents a graphical representation of the RCS surfaces of the large plane target.

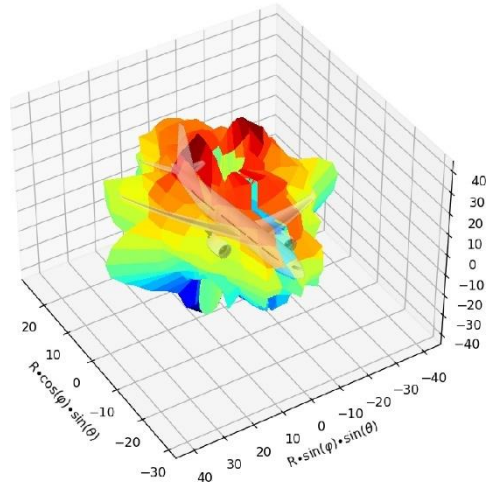

Fig. 7. Diagram of the Radar Cross Section of a large plane type target, at a frequency of 10 MHz, horizontal polarization.

C. Kinematic Array

This model allows evaluating and determining how the position and velocity of the targets evolves over time (see Fig. 8). The possible trajectories they can describe are rectilinear or curvilinear.

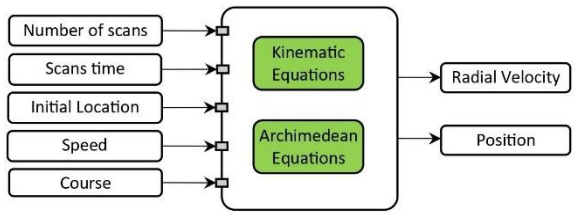

Fig. 8. Kinematic Model of the Targets. Input and output parameters.

An *x*, *y*, *z* coordinate system is used, where the origin matches the location of the radar (See Fig, 9). The variables correspond to latitude, longitude, and altitude, respectively.

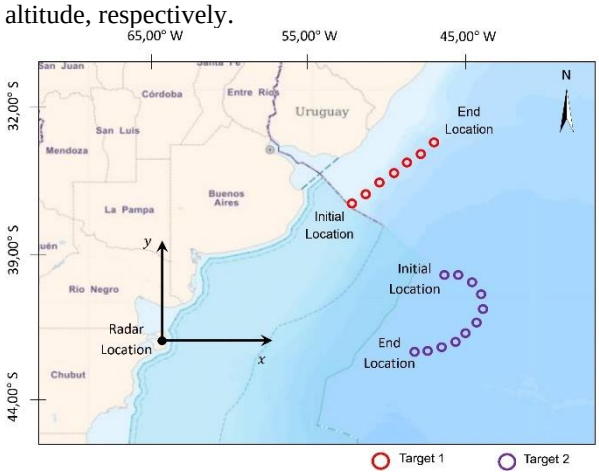

Fig. 9. Representation of the chosen coordinate system, along with an example of the straight and curved trajectories followed by the targets.

For straight trajectories, the determination of the next state of movement in the *x*, *y* plane is based on the equations of classical kinematics for uniform rectilinear motion.

For curved trajectories, the determination of the next state of movement in the *x*-*y* plane is based on the equations of the Archimedean spiral, which in turn is based on polar coordinates.

Finally, the conversion from polar coordinates to rectangular coordinates must be carried out to represent the trajectory in the selected coordinate system. For simplification purposes, the target moves describing the curved trajectory with constant speed.

To determine the positions that the target acquires in its "*z*" axis, which represents the altitude, we used the multipath fading effect based on Earth curvature model [6].

D. Antenna Array Model

This model simulates the behaviour of antennas *arrays*, as the interaction of many individual radiators distributed on a surface that conform either the transmitter or the receiver.

The user can setup the following parameters for each of the arrays: number of elements, geometry type (rectangular, circular, and star), physical separation between elements, radiation pattern of elements (quarter-wave dipole or isotropic radiator) and working frequency.

The array model is presented in Fig. 10.

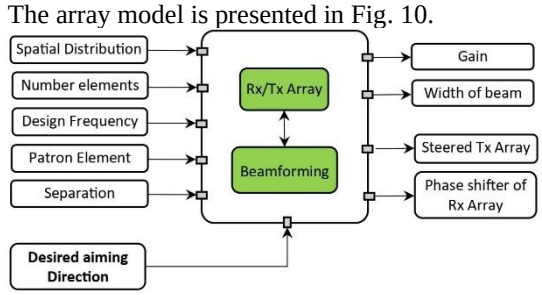

Fig. 10. Transmitter and Receiver antenna array model.

After both the user input and the aiming direction have been defined, the model is able to steer the main lobe of the transmitting array through beamforming techniques. The desired aiming direction is obtained from the Ray Parameters model.

On the other hand, the receiving array simulates the spatial phase shift of the signal received by each element as it propagates through the array. This phase shift information is later used by the Signal Generation model and the Processing Digital Signal model for estimating angle of arrival. Fig. 11 presents three examples of steered transmission arrays.

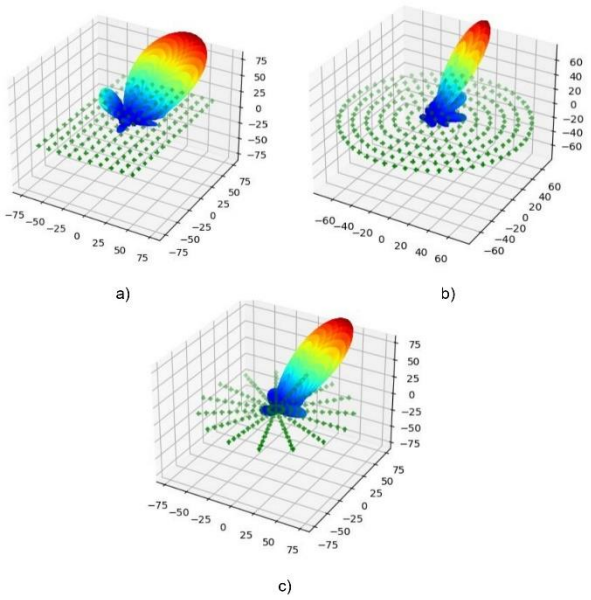

Fig. 11. Transmission arrays with 150 elements with rectangular (a), circular (b), and star distributions (c). Arrays oriented in elevation and azimuth: φ=60 °, θ=20 °.

E. Ray Parameters Model

This model determines the characteristics that an electromagnetic wave must have to achieve propagation in the Earth's ionosphere, between an initial point (radar position) and final point (target position) located on the surface of the Earth or sea. The characteristics of the wave are the frequency, aiming direction, delay, ranges, and propagation attenuation.

The model is composed of two submodels: an analytical ray tracer and an ionosphere modeler, both presented in Fig. 12.

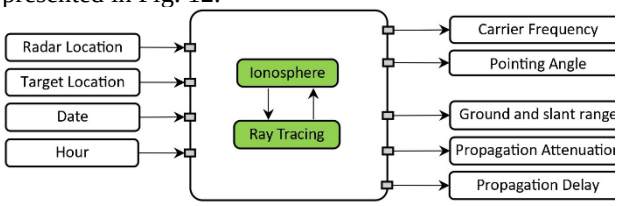

Fig. 12. Ray Parameters Model. Input and output parameters, submodels of Earth's Ionosphere and Ray Tracer.

1) Ionosphere Model

The ionosphere model is based on the International Reference Ionosphere model IRI-2012 [7]. The IRI model is the result of the efforts of the scientific community who have worked over the last 60 years to improve and update a standard model of the Earth's ionosphere. This is a complex empirical model that determines different values of the ionosphere state. The most relevant for this study are electron density, critical frequency and peak height of the layers, semi-thickness and composition. These parameters are function of geographic coordinates, date and time; which in turn define the solar activity level on which the ionosphere strongly depends.

2) Ray Tracing Model

The ray tracer allows, based on the frequency and direction of an electromagnetic wave, to determine its propagation path within the medium formed by the ionosphere and the lower layers of the troposphere, stratosphere, and mesosphere. An example of the propagation path of a wave determined by the tracer is presented in Fig. 13. The model is based on a system of equations that analytically determine parameters such as: group and phase delay, terrestrial and oblique range reached by the wave [8].

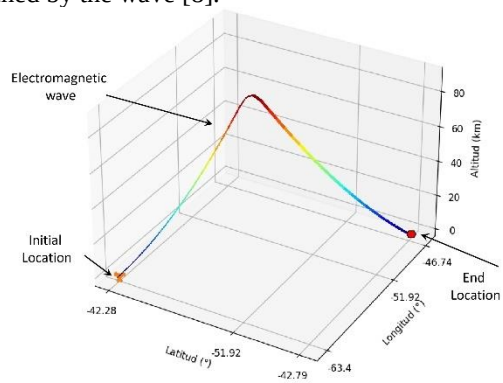

Fig. 13. Example of the path followed by an electromagnetic wave between two points on the Earth's surface.

F. Received Signal Characterization Model

The characterization model determines parameters of the signal received by the receiving system after the electromagnetic wave has interacted with the medium and the proposed scenario. This is important to later generate signals based on the parameters obtained in this stage.

The received signal is modelled according to the following equation.

$$S_R = Echo + Noise + Clutter. \quad (1)$$

Where S_R is the received signal, *Echo* is the signal reflected by the targets of interest, *Noise* is an unwanted random signal coming from the surroundings of the antenna arrays and *Clutter* corresponds to the undesired reflection of electromagnetic energy in the surroundings of the targets. For this study, the sea is the Clutter source.

The parameters of interest for the received signal are amplitude levels, frequency, and phase. The

https://mc.manuscriptcentral.com/taes

mathematical models and equations used in the radio link model can be found in [9][10]. Figure 14 presents a block diagram with the submodels that determine each of the parameters of S_R.

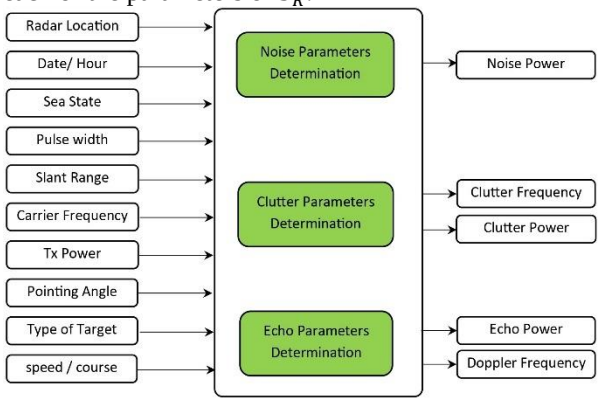

Fig. 14. Model of characterization of the received signal. Input and output parameters, submodels for determining parameters of Noise, Clutter, and Echo.

G. Signal Generation Model

This model is responsible for generating time series of n samples corresponding to the signal received by an antenna array of k elements during a coherent integration interval of m pulses. These are treated as a three-dimensional matrix $\boldsymbol{M}$ $(n \times m \times k)$ for subsequent processing.

Figure 15 shows the block diagram of the signal generator. The simulator is based on a mono-static *pulsed* radar system, where transmission and reception take place at different time intervals.

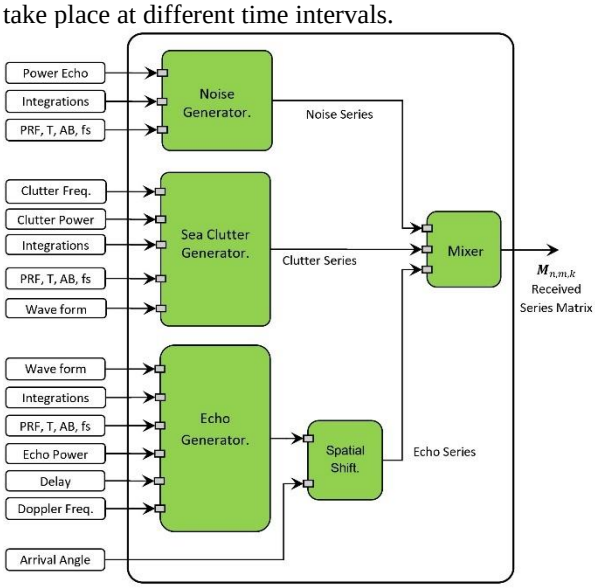

Fig. 15. Received Signal Generation Model. Input and output parameters.

In the model, there are three generators:

- Noise Generator: generates a time series of n samples, based on pulse repetition frequency (PRF) and sampling frequency (f_s). For the amplitude, we use Log-Normal probability distribution function with the average level coming from the Characterization model. The generation of this series is repeated m times, m being the number of integrations.
- Echo Generator: generates a time series of n samples based on PRF, pulse width (T), bandwidth (AB), and sampling frequency. A delay is added to represent the time it takes for the wave to propagate the full round trip (from transmitter to receiver). Additionally, the Doppler Frequency associated with the target's state of motion influences the carrier frequency present in the series. For the amplitude, we use Swerling I-II-III-IV probability distribution function with the average level coming from the Characterization model. The generation of this series is repeated m times, m being the number of integrations.
- Clutter Generator: generates a time series of n samples based on PRF, pulse width, bandwidth, and sampling frequency. For this study we only consider the sea clutter, which is the result of electromagnetic energy impacting the sea surface. This interaction is represented with two spectral lines on each side of 0 Hz. For the amplitude, we use Rayleigh or K probability distribution function with the average level coming from the Characterization model. The generation of this series is repeated m times, m being the number of integrations.

On the other hand, after the Echo series is generated, it enters a Spatial Phase Shifter which models the *reception* of the signal by an antenna array of k elements, where there is a spatial phase shift between the signals received by each antenna element. The phase shift is based on the arrival direction of the signal and the spatial distribution of the receiving antenna array, which can be rectangular, star, and circular.

Finally, the Combiner is responsible for combining the time series of noise, clutter, and echo to obtain the $\boldsymbol{M}$ matrix corresponding to the received signal.

H. Signal Generation Model

This module is responsible for applying various methods and digital data processing techniques to the $\boldsymbol{M}$ matrix of received signal samples, with the aim of

https://mc.manuscriptcentral.com/taes

extracting range, arrival direction, and Doppler frequency information of potential targets present in the received signals. The block diagram of the processing module is presented in Fig. 16.

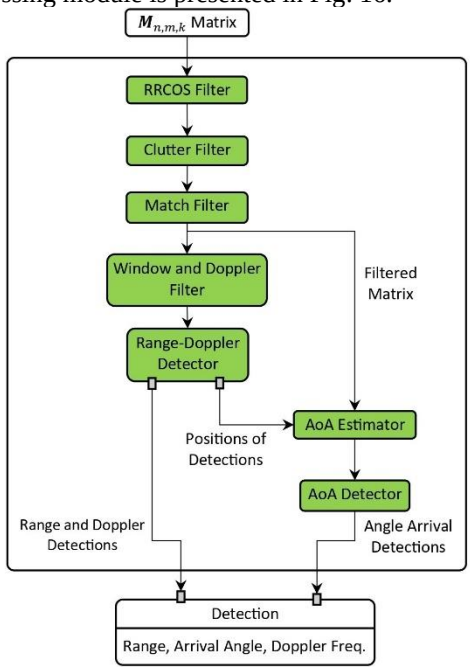

Fig. 16. Digital signal and data processing module.

The tasks performed by each of the blocks are described below.

1) **Raised Root Cosine Filter**

This filter helps reduce the inter-symbol interference produced in the transmission channel. This phenomenon occurs because the signal is modulated with binary codes at the transmitting stage. The filter is applied in the sample domain (along the *n*-axis of the ***M*** matrix).

2) **Clutter Filter**

This is responsible for removing the clutter part from the received signal. For this work, the exploration area is always surrounded by the sea. In this case, the energy received is mainly due to the reflections on the sea, as it has greater cross section area than the targets combined, if any [11].

For this purpose, we use the Empirical Mode Decomposition (EMD) technique [12]. This method allows decomposing the signal into its most significant components. We can associate clutter signal to these main components and then filter it out from the received signal. The filter is applied in the sample domain (along the n-axis of the ***M*** matrix).

3) **Matched Filter**

This simulator simulates a radar operating under a compressed pulsed mode. This is a very common technique in radar systems to significantly increase SNR figure [13][14]. It relies on (a) encoding the phase of the transmitting signal with some code that optimizes its detection when received, and (b) applying a correlation mechanism on the received signal that detects the presence of the encoded information.

This filter is used for the latter task. It implements the correlation function between the received signal and a copy of the transmitted signal, detecting the *autocorrelation*. The purpose of this operation is to highlight the delay present between the transmitted signal and the echo signal (signal of interest) present in the received signal. This filter is applied in the sample domain (along the *n*-axis of the ***M*** matrix).

After applying the filter to the ***M*** matrix, the axis (*n*) domain is transformed from samples to range by multiplying each sample by the vacuum speed of light value and dividing by 2, This number is because the determined time considers the round-trip path.

4) **Window and Doppler Filter**

When processing the signal to extract Doppler information (see Doppler Filter) for velocity retrieval, the raw data is segmented into rectangular windows. This introduces significant sidelobes in the frequency domain. To mitigate this problem, the Kaiser-Bessel window is applied before the Doppler filtering. This windowing technique smooths the data and discontinuities at its edges, effectively reducing the sidelobes and resulting in cleaner spectrum for the Doppler filter stage [15]. This filter is applied in the pulse domain (along the *m*-axis of the ***M*** matrix).

On the other hand, the Doppler filter is designed to estimate the relative velocities of detections. When a radar wave bounces off a moving target, the returned signal's frequency changes. The Doppler effect highlights this frequency shift, which is proportional to the object's velocity relative to the radar.

This filter is implemented using Fast Fourier Transform in the pulse domain (along the *m*-axis of the ***M*** matrix). The output is a spectrum where the Doppler frequency components associated with the signal of interest (echo signals) are observed [16].

Finally, we transform the *pulse* axis to *Doppler frequency* axis. The resulting ***M*** matrix axis are *range (m)*, *Doppler Frequency (n)* and *number of elements (k)*.

5) **Range-Doppler Detector**

The spectrogram obtained from the Doppler Filter shows how much the received signal is alike the transmitted one. This correlation progressively decays

around points of local maxima. An *adaptive detector* is used to detect these points, which are potentially due to the presence of a target.

This stage is implemented using a *Cell Averaging Constant False Alarm Rate* (*CA-CFAR*) detector in two dimensions with a modified refence window: over the *range (m)* and *Doppler Frequency (n)* domains [17].

6) **Angle of Arrival Estimator**

Determines the arrival direction/angle of the received signals with respect to the receiving antenna array. The applied method is called Propagator Direct Data Acquisition (PDDA) [18]. This method is applied in the sample and element domains (along the *n* and *k* axes of the ***M*** matrix).

The method uses the positions detected (along the range axis) by the Range-Doppler detector as input along with the ***M*** matrix filtered by the matched filter. The information from the previously detected positions is used to focus the search on positions where there is already prior knowledge of the possibility of the existence of a potential target echo. After applying this method, the element axis (*k*) of the ***M*** matrix transforms into the angle of arrival axis.

In this point the dimensions of the ***M*** matrix are *n* = range, *m* = Doppler Frequency and *k* = arrival angle.

7) **Angle of Arrival Detector**

After applying the angle of arrival estimator, angle spectrograms (theta and phi) associated with the search area are obtained. The detector allows identifying possible targets within the DIR area and also obtaining phi angle (azimuth) and theta (elevation) values from the spectrograms. The detector is of the adaptive type, in particular, the CA-CFAR in two dimensions. This data processing technique is applied over the range and arrival angle domains (along the *n* and *k* axes of the ***M*** matrix).

Finally, after applying the entire processing chain, a set of detections characterized by range, arrival direction, and Doppler frequency values are obtained, which are suspected to belong to the echoes of targets present in the search area.

I. Radar-to-Geographic Parameters Conversion Module

This module is responsible for transforming the values of range, arrival angle, and Doppler frequency into geographical position and radial speed of the detections (see Fig. 17).

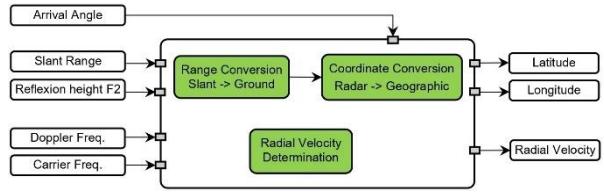

Fig. 17. Radar-to-Geographic Parameter conversion module. Input and output parameters.

The Range Conversion module uses a set of equations to convert the oblique range, which is the propagation path followed by the electromagnetic wave in its full round trip, into ground range, which is the projection of the oblique range onto the earth's surface.

The Coordinate Conversion allows the transformation of radar relative coordinates (ground range and direction) into geographical coordinates (latitude and longitude).

On the other hand, radial speed is determined by multiplying Doppler frequency by the vacuum speed of light value and dividing by carrier frequency of the transmitted signal.

J. Detection Output

The output detections are saved to both an interactive map and a plain table (*csv* file). This tool specifically saves the following files after each exploration:

- ***params.json***: all the parameters setup by the user for this run.
- ***datos_cinematica.csv***: position and speed information for every target set up in the proposed scenario.
- ***mapa_con_detecciones.html***: interactive geographic map for viewing proposed scenario and output detections (see Fig. 18).
- ***resultados.csv***: plain table of output detections.

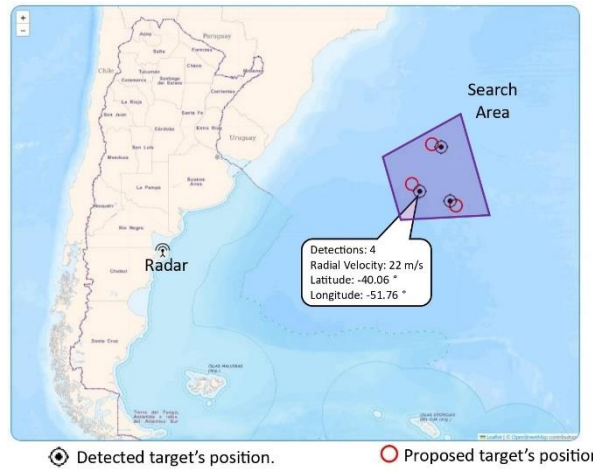

https://mc.manuscriptcentral.com/taes

Fig. 18. Visualization of the detections found, in the User Interface of the simulator (OTHR-SW).

III. RESULT

In this section, we choose a specific radar configuration and evaluate it against two search scenarios:

- Scenario 1: A single target navigating a curved path, with movements towards and away from the radar and points where the radial velocity is null even while in motion.
- Scenario 2: Features multiple targets each pursuing a distinct linear trajectory, operating independently of one another.

The radar system settings, antenna locations, and the search area remain the same across scenarios. The antenna systems have star geometry, comprises 150 elements, and are located in Chubut, Argentina. The center of the DIR exploration region is located about 1000 km to the east and extends to approximately 1500 km. This represents roughly half the range of these types of radars [19]. We varied the targets quantity and motion and the exploration configuration.

A. Scenario 1

In this case study, we focus on evaluating the OTH-SW simulation tool for positive, negative, and near-zero radial velocity values.

For this, we designed a scenario where a Cargo Ship, being the only target, follows a curved path at constant speed, as illustrated in Fig. 19. This target is be scanned in this simulation, 15 times at intervals of 16 minutes.

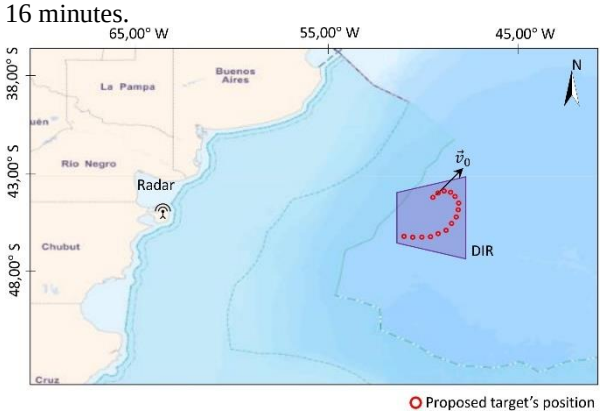

Fig. 19. Representation of the radar system positions, search area, and the target's trajectory.

Tables 1, 2, and 3 detail the parameters configured for: proposed scenario, exploration, and radar system.

TABLE I
Configuration of proposed scenario.

Proposed Scenario Setting	
Search Area	**Value**
Radar Location	42.55 ° S 63.83 ° W
DIR Location	42.70 ° S 51.46 ° W
Target	**Value**
Type	Panama-like
Initial Course	20 °
Initial Speed	11,8 m/s
Path	Curl
Initial Location	42.04° S 51.49° W
Environment	**Value**
Ionosphere State	Calm
Sea State	Moderate (Wave height 1.25 to 2.5 m)
Zone Type	Rural
Date And Hour	2005-05-15T16.00

TABLE II
Configuration of explorations.

Exploration Settings	
Scans	**Value**
Period	16 min
Number of scans	15
Tx Signal	**Value**
Operation mode	Pulsed-Coded
Bandwidth	10 kHz
PRF	40 Hz
Power	40 dBW
Sample Freq.	30 kHz
Code Type	Barker 11
Digital Processing	**Value**
Range-Doppler Detector (Pfa)	$7.0\ 10^{-3}$
Arrival Angle Detector (Pfa)	$4.0\ 10^{-3}$

TABLE III
Configuration of radar.

Radar System Settings	
Antenna Arrays (Tx and Rx)	**Value**
Geometry	Star
Elements	150
Spacing	0.15 λ
Design Freq.	50 MHz

https://mc.manuscriptcentral.com/taes

Base pattern	λ/4 dipole
Receiver	**Value**
Signal Gain	250 dB
SNR	40 dB
SCR	20 dB
Inter. Freq.	0.0 Hz
Bandwidth	30 MHz

After setting all parameters, we proceeded with the simulation. Table 4 shows the target's temporal evolution, produced by the Kinematics module. These are the values the tool should identify at the simulation's end. The estimated and proposed values for *(i)* geographic position and *(ii)* radial velocity are shown in Figures 20 and 21, respectively.

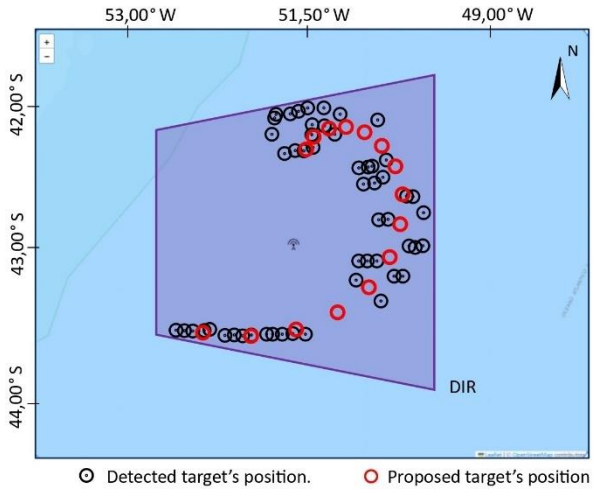

Fig. 20. Detected (in black) and proposed (in red) target positions over the 15 scans.

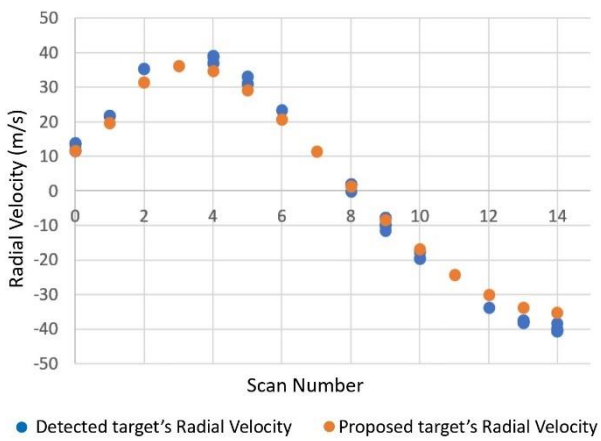

Fig. 21. Detected (in blue) and proposed (in orange) target radial velocity over the 15 scans.

It is important to emphasize that the configuration of the CFAR detector will significantly influence the number of positive detections recorded, due to its relationship with the false alarm probability. Here we proposed a single target, so we attribute all recorded detections to it. Finally, when calculating the errors, we use the worst of the estimated values for each exploration. The detailed results of this approach can be observed in Table 5, where the errors found in the detections are shown.

TABLE IV

Temporal evolution of the position and radial velocity of the proposed target over the 15 scans.

Proposed Target's Motion		
Scan Nº	**Geographical Location (Lat, Lon)**	**Radial Velocity**
0	42.04° S, 51.49° W	11.8 m/s
1	41.94° S, 51.41° W	19.8 m/s
2	41.89° S, 51.27° W	31.3 m/s
3	41.87° S, 51.10° W	36.2 m/s
4	41.92° S, 50.92° W	34.8 m/s
5	42.02° S, 50.75° W	29.2 m/s
6	42.17° S, 50.62° W	20.9 m/s
7	42.36° S, 50.55° W	11.3 m/s
8	42.59° S, 50.56° W	1.4 m/s
9	42.82° S, 50.67° W	-8.2 m/s
10	43.04° S, 50.88° W	-16.9 m/s
11	43.22° S, 51.19° W	-24.3 m/s
12	43.35° S, 51.58° W	-30.0 m/s
13	43.40° S, 52.04° W	-33.8 m/s
14	43.36° S, 52.53° W	-35.2 m/s

TABLE V

Maximum absolute and relative errors of position and radial velocity. The errors are calculated between the estimated values from the detections and the proposed target values.

Max. Estimated Error		
Scan Nº	**Absolute error Geographical Location**	**Relative error Radial Velocity**
0	39.77 km	0.17
1	40.91 km	0.10
2	30.44 km	0.13
3	No detections	No detections
4	28.04 km	0.12
5	33.01 km	0.13
6	6.30 km	0.12
7	No detections	No detections
8	36.98 km	0.41
9	50.45 km	0.18
10	39.31 km	0.16

11	61.85 km	No detections
12	18.73 km	0.12
13	55.77 km	0.13
14	44.45 km	0.15

In summary, in this case study, the OTH-SW simulation tool was able to track the target adequately along its trajectory, identifying positive, negative, and near-zero radial velocity values.

B. Scenario 2

In this case study, we explore the interactions of three independent targets, each following a straight trajectory. We focus on the evaluation of *simultaneous* detections of all targets, for positive, negative and near-zero radial velocities.

The proposed scenario includes two fishing vessels and a commercial airplane moving on independent trajectories and being explored 10 times at intervals of 13 minutes. The design is illustrated in Fig. 22.

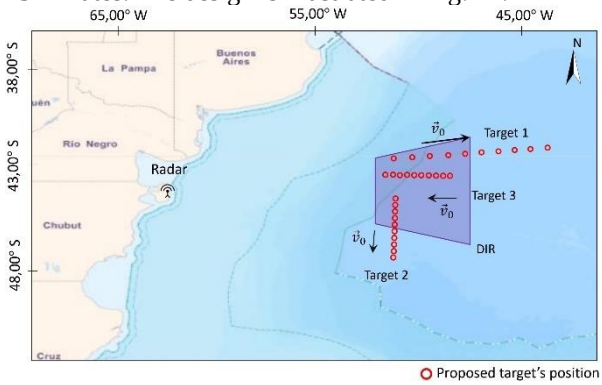

Fig. 22. Representation of the radar system positions, search area, and the trajectory of three targets.

Tables 6, 7, and 8 detail the parameters configured for: proposed scenario, exploration, and radar system.

TABLE VI
Configuration of the proposed scenario.

Proposed Scenario Setting	
Search Area	**Value**
Radar Location	42.55 ° S 63.83 ° W
DIR Location	42.70 ° S 51.46 ° W
Target 1	**Value**
Type	Commercial Aircraft
Initial Course	90 º
Initial Speed	200 m/s
Path	Stright
Initial Location	41.70° S 52.43° W
Target 2	**Value**
Type	Fishing Vessel
Initial Course	180 º
Initial Speed	20 m/s
Path	Stright
Initial Location	43.32° S 52.58° W
Target 3	**Value**
Type	Fishing Vessel
Initial Course	270 º
Initial Speed	40 m/s
Path	Stright
Initial Location	42.68° S 53.09° W
Environment	**Value**
Ionosphere State	Calm
Sea State	Moderate (Wave height 1.25 to 2.5 m)
Zone Type	Rural
Date And Hour	2005-05-15T16.00

TABLE VII
Configuration of exploration.

Exploration Settings	
Scans	**Value**
Period	13 min
Number of scans	10
Tx Signal	**Value**
Operation mode	Pulsed-Coded
Bandwidth	10 kHz
PRF	40 Hz
Power	40 dBW
Sample Freq.	30 kHz
Code Type	Barker 13
Digital Processing	**Value**
Range-Doppler Detector (Pfa)	$1.0\ 10^{-3}$
Arrival Angle Detector (Pfa)	$4.0\ 10^{-4}$

TABLE IIX
Configuration of Radar.

Radar System Settings	
Antenna Arrays (Tx and Rx)	**Value**
Geometry	Star
Elements	150
Spacing	0.15 λ
Design Freq.	50 MHz
Base pattern	λ/4 dipole

https://mc.manuscriptcentral.com/taes

Receiver	Value
Signal Gain	250 dB
SNR	40 dB
SCR	20 dB
Inter. Freq.	0.0 Hz
Bandwidth	30 MHz

After the initialization of the parameters, we executed the simulation. Tables 9a, 10a and 11a show the temporal evolution of each target, determined by the Kinematics module. These are the values that the tool should recognize at the end of the simulation. Fig. 23 showcase estimated vs. proposed values of geographic position.

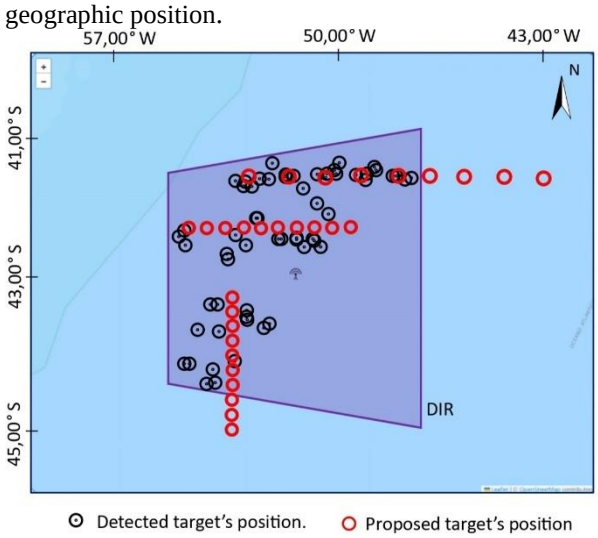

Fig. 23. Detected (in black) and proposed (in red) target positions over the 10 scans.

To address the problem of mapping each detection to each target, we used radial velocity as the main grouping criterion, a strategy illustrated in Fig. 24. Then, in Fig. 25, we compare the proposed radial velocities with those derived from the detections.

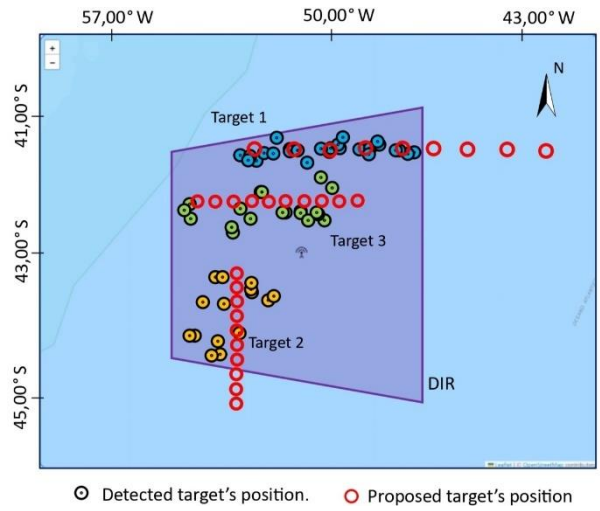

Fig. 24. Detected (in black) and proposed (in red) positions of the three targets over the 10 scans.

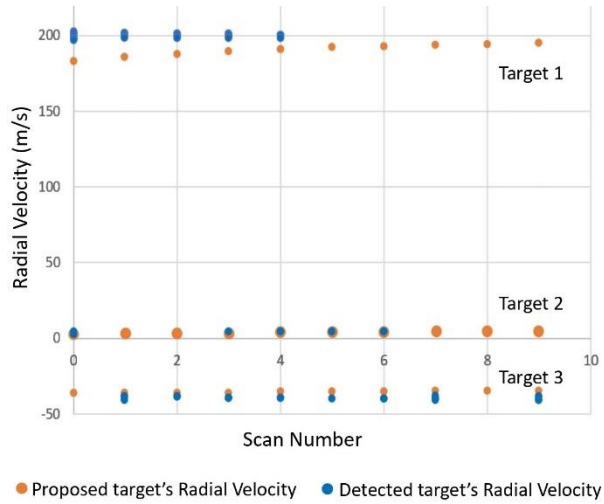

Fig. 25. Detected (in black) and proposed (in red) radial velocity of the three targets over the 10 scans.

Similar to Scenario 1, we took the largest difference found in each exploration to determine the errors in latitude, longitude, and velocity. The most significant errors are detailed in Tables 9b, 10b, and 11b.

In summary, this case study demonstrated that the OTH-SW simulation tool can successfully identifies and follows each target along its respective trajectory, accurately discerning the variations in radial velocities and geographic locations, considering the maximum errors. Thus, this scenario corroborates the tool's ability to handle complex scenarios with multiple targets moving on independent straight trajectories.

https://mc.manuscriptcentral.com/taes

TABLE IX

(a) Temporal evolution for Target 1 (Commercial airplane) from Kinematics module. (b) Absolute and relative maximum error for each scan.

Target 1	Proposed Target's Motion		Max. Estimated Error	
Scan Nº	Geographical Location (Lat, Lon)	Radial Velocity	Absolute error Geographical Location	Relative error Radial Velocity
0	41.70 ° S, 52.43 ° W	182.88 m/s	53.98 km	0.106
1	41.70 ° S, 51.35 ° W	185.69 m/s	34.50 km	0.087
2	41.70 ° S, 50.28 ° W	187.74 m/s	37.54 km	0.071
3	41.70 ° S, 49.20 ° W	189.50 m/s	37.48 km	0.060
4	41.70 ° S, 48.12 ° W	190.89 m/s	92.64 km	0.049
5	41.70 ° S, 47.04 ° W	191.96 m/s	No detections	No detections
6	41.70 ° S, 45.96 ° W	192.93 m/s	No detections	No detections
7	41.70 ° S, 44.89 ° W	193.58 m/s	No detections	No detections
8	41.70 ° S, 43.81 ° W	194.17 m/s	No detections	No detections
9	41.70 ° S, 42.73 ° W	194.62 m/s	No detections	No detections

TABLE X

(a) Temporal evolution for Target 2 (Fishing Vessel) from Kinematics module. (b) Absolute and relative maximum error for each scan.

Target 2	Proposed Target's Motion		Max. Estimated Error	
Scan Nº	Geographical Location (Lat, Lon)	Radial Velocity	Absolute error Geographical Location	Relative error Radial Velocity
0	43.32 ° S, 52.58 ° W	2.79 m/s	132.26 km	0.445
1	43.43 ° S, 52.58 ° W	3.02 m/s	49.36 km	0.327
2	43.53 ° S, 52.58 ° W	3.24 m/s	No detections	No detections
3	43.64 ° S, 52.58 ° W	3.46 m/s	28.10 km	0.164
4	43.74 ° S, 52.58 ° W	3.67 m/s	48.97 km	0.111
5	43.84 ° S, 52.58 ° W	3.88 m/s	49.38 km	0.045
6	43.95 ° S, 52.58 ° W	4.10 m/s	127.27 km	0.019
7	44.05 ° S, 52.58 ° W	4.31 m/s	No detections	No detections
8	44.15 ° S, 52.58 ° W	4.53 m/s	No detections	No detections
9	44.26 ° S, 52.58 ° W	4.74 m/s	No detections	No detections

TABLE XI

(a) Temporal evolution for Target 3 (Fishing Vessel) from Kinematics module. (b) Absolute and relative maximum error for each scan.

Target 3	Proposed Target's Motion		Max. Estimated Error	
Scan Nº	Geographical Location (Lat, Lon)	Radial Velocity	Absolute error Geographical Location	Relative error Radial Velocity
0	-42.69 ° S, 50.51 ° W	-36.40 m/s	No detections	No detections
1	-42.69 ° S, 50.80 ° W	-36.23 m/s	46.58 km	0.076
2	-42.69 ° S, 51.08 ° W	-36.07 m/s	32.71 km	0.082
3	-42.69 ° S, 51.37 ° W	-35.89 m/s	31.44 km	0.094
4	-42.69 ° S, 51.66 ° W	-35.78 m/s	25.67 km	0.104
5	-42.69 ° S, 51.95 ° W	-35.50 m/s	39.59 km	0.129
6	-42.69 ° S, 52.23 ° W	-35.37 m/s	26.48 km	0.131
7	-42.69 ° S, 52.52 ° W	-35.07 m/s	102.74 km	0.094
8	-42.69 ° S, 52.81 ° W	-34.82 m/s	No detections	No detections
9	-42.69 ° S, 53.10 ° W	-34.59 m/s	29.57 km	0.129

IV. DISCUSSION AND CONCLUSION

Throughout this research, we have developed a simulation tool tailored for the preliminary design and assessment of OTH-SW radar systems. This tool excels by consolidating, within a single platform, a range of functionalities that were previously fragmented across existing literature. It not only embodies capabilities previously explored but takes a step further, modelling additional phenomena and interactions that allow a broader and more accurate evaluation of various radar configurations.

The scenarios outlined in the results section showcase the simulator's ability to *reproduce* real-world conditions with acceptable fidelity, and *detect* positive, negative and near-zero radial velocities; even when multiple targets are present. This translates into a powerful instrument for the preliminary validation of radar configurations, a crucial step towards the construction of *viable* radar systems. With minimal adaptations, the PDS module then can be used an operative radar.

Looking forward, we identify several promising routes to further expand our tool's capabilities. Two upcoming features we are considering are:

- Machine learning techniques for automatic determination of configuration parameters. This should significantly ease the number of iterations needed to arrive at local optimal results.
- Target segmentation and tracking, to identify any number of simultaneous targets present in an exploration region. This should significantly reduce redundant detections and should also allow the prediction of subsequent positions.

Additionally, we highlight the interest expressed by the Argentine Air Force in incorporating our simulator into their Simulation and War Games Center [20], a meaningful validation of the practical and applied potential of our tool.

In conclusion, we have presented an innovative resource that facilitates not only theoretical evaluation but also practical implementations in the field of OTH-SW radars, fostering a pathway for faster and more accurate developments.

APPENDIX

In this appendix, we detail the configurable parameters available in the OTH-SW simulator, categorized into three distinct groups for ease of understanding and management.

The first group encompasses parameters pertaining to the radar configuration itself, delineating the various settings that representing a *constructed* radar, such as location, geometry and electrical characteristics. **Radar system** parameters and their descriptions are shown in Table A.1.

Following this, the second group delineates the parameters that shape the proposed scenario; including the targets present within the search area as well as the environmental ionosphere and sea conditions that will interfere with the signal. **Proposed scenario** parameters and their descriptions are shown in Table A.2.

The final group of exploration parameters delineates how the tool will configure and handle the signal both before transmitting and after receiving. This encapsulates operational choices such as modulation, pulse repetition frequency, and false alarm rates. **Exploration** parameters and their descriptions are shown in Table A.3.

TABLE A1

Radar system configurable parameters and their descriptions.

Radar System Parameters	
Array Antenna Tx, RX	**Description**
Geometrical Distribution	Geometrical distribution of antenna array (rectangular, circular, star)
Number of elements	Number of antennas of array
Element spacing	Inter-element spacing in unit of wavelength.
Design Freq.	Design Frequency of array.
Type antenna	Type of individual antenna (isotropic, quarter wave dipole).
Receiver	**Description**
Signal Gain	Signal power gain.
SNR	Receiver output Signal-to-Noise Rate.
SCR	Receiver output Signal-to-Clutter Rate.
Inter. Freq.	Intermediate frequency of receiver
Bandwidth	Bandwidth of receiver

TABLE A2
Proposed scenario configurable parameters and their descriptions.

Proposed Scenario Parameters	
Search Area	**Description**
Radar Geog. Location	Radar system Geographical Location (Latitude, Longitude)
DIR Geog. Location	Dwell Illumination Region çGeographical Location (Latitude, Longitude)
Target	**Description**
Type	Type of target (ships or aircraft)
Initial Course	Initial course of target (geographical azimuth).
Initial Speed	Initial speed of target.
Path	Type of path followed by the target (curve, straight).
Geographical Location	Initial Geographical Location of target (Latitude, Longitude).
Environment	**Value**
Ionosphere State	Ionosphere state (With, without disturbances). In this version only "without" is available.
Sea State	Sea state (0 - 9). 0: Calm (glassy) and 9: Phenomenal (Hurricane).
Type zone	Type zone where is located of radar system (city, residential, rural, quiet).
Date and Hour	Date and time of start search target.

TABLE A3
Exploration configurable parameters and their descriptions.

Exploration Parameters	
Scans	**Description**
Period	Time interval between scans.
Number of scans	Number of scans over a DIR area.
Tx Signal	**Description**
Operation Mode	Mode of Operation del radar (Pulsed-modulated, Continuous).
Bandwidth	Bandwidth of the transmitted signal.
PRF	Pulse of Frequency Pulse.
Power	Power average of transmitted signal.
Sample Freq.	Sampling frequency for signal generation.
Carrier Freq.	Carrier frequency of transmitted signal.
Code Type	Code used for modulation.
Pulse width	Width of transmitted pulse.
Digital Processing	**Description**
Pfa Range-Doppler	Probability of false alarm used for Range-Doppler detector.
Pfa Arrival Angle Detector	Probability of false alarm used for Arrival Angle detector.

REFERENCES

[1] G. A. Fabrizio Introduction In *High frequency over-the-horizon radar*, 1st ed., New York, USA, McGraw Hill, 2013, pp. 11- 20.

[2] M. Feng *et al.* Research on a simulation model of a skywave over-the-horizon radar sea echo spectrum *Remote Sens.*, vol.14, no 6, pp. 1461, 2022, doi:10.3390/rs14061461.

[3] W. Sun, M. Ji, W. Huang, Y. Ji and Y. Dai vessel tracking using bistatic compact HFSWR *Remote Sens.*, vol. 12, pp .1266, 2020, doi: 10.3390/rs12081266.

[4] M.A. Cervera, D. B. Francis and G. J. Frazer Climatological model of over-the-horizon radar *Radio Science*, vol. 53, pp. 988–1001, 2018, doi: 10.1029/2018RS006607.

[5] Y. Zhu, Y. Wei and Y. Li First order sea clutter cross section for hf hybrid sky-surface wave radar *Radioengineering*, vol. 23, no.4, pp. 1180-1191, 2014.

[6] C. Hou, Y. Wang, and J. Chen Estimating target heights based on the earth curvature model and micromultipath effect in skywave OTH radar *Journal of Applied Mathematics*, vol. 2014, Article ID 424191, pp. 1-14, 2014, doi: 10.1155/2014/424191.

[7] D. Bilitza *et al.* The international reference ionosphere 2012 - a model of international collaboration *Journal of Space Weather and Space Climate*, vol. 4, pp. 1–12, 2014, doi: 10.1051/swsc/2014004.

[8] T. A. Croft and H. Hoogansian Exact ray calculations in a quasi-parabolic ionosphere with

no magnetic field *Radio Science*, vol. 3, no.1, 1968, doi: 10.1002/rds19683169.

[9] Z. Saavedra, D. Zimmerman, M. A. Cabrera and A. G. Elias Sky-wave over-the-horizon radar simulation tool *IET Radar Sonar Navig.*, vol. 14, pp. 1773-1777, 2020, doi: 10.1049/iet-rsn.2020.0158.

[10] Z. Saavedra Modelado del canal de propagación de un radar sobre horizonte Ph.D. thesis, Dept. Electric., Electron. and Compu. Tucumán Nacional Univ., Tucumán, Argentina, 2020, https://www.facet.unt.edu.ar/posgrado/wp-content/uploads/sites/54/2022/11/Tesis_ZSaavedra_2020.pdf.

[11] R. H. Khan Ocean-clutter model for high-frequency radar, *IEEE J. Ocean Eng*., vol. 16, no. 2, pp. 181–188, 1991, doi: 10.1109/48.84134.

[12] I. Mostafanezhad, O. Boric-Lubecke, V. Lubecke and D. P. Mandic Application of empirical mode decomposition in removing fidgeting interference in doppler radar life signs monitoring devices In *Annu. Int. Conf. IEEE Eng. Med. Bio. Soc.*, Minneapolis, MN, USA, 2009, pp. 340-343, doi: 10.1109/IEMBS.2009.5333206.

[13] N. J. Mohamed Nonsinusoidal radar signal design for stealth targets In *IEEE Transactions on Electromagnetic Compatibility*, vol. 37, no. 2, pp. 268-277, 1995, doi: 10.1109/15.385893.

[14] M. A. Cabrera *et al.* Some considerations for different time-domain signal processing of pulse compression radar *Annals of Geophysics*, vol. 53, pp. 5-6, 2010, doi: 10.4401/ag-4758.

[15] A. V. Oppenheim and R. W. Schafer Filter design Techniques In *Discrete-time signal processing*, 2nd ed., New Jersey, USA, Prentice Hall, 1998, pp. 474 - 485.

[16] K. Don How to create and manipulate radar range–doppler plots Def. Sci. Tech. Org., Australia, Tech. Rep. DSTO-TN-1386, Dec. 2014.

[17] W. Wang, R. Wang, R. Jiang, H. Yang and X Wang Modified reference window for two-dimensional CFAR in radar target detection *The Journal of Engineering*, 2019, doi: 10.1049/joe.2019.0687.

[18] M. A. G. Al-Sadoon *et al.* A New Low Complexity Angle of Arrival Algorithm for 1D and 2D Direction Estimation in MIMO Smart Antenna Systems *Sensors*, vol. 17, 2017, doi: 10.3390/s17112631.

[19] G. A. Fabrizio Introduction In *High frequency over-the-horizon radar*, 1st ed., New York, USA, McGraw Hill, 2013, pp. 39 - 41.

[20] CSJG, Centro de Simulación y Juegos de Guerra *Dirección General de Investigación y Desarrollo de la Fuerza Aérea Argentina*, 2023, Argentina. https://www.argentina.gob.ar/fuerzaaerea/direccion-general-de-investigacion-y-desarrollo/centro-de-simulacion-y-juegos-de-guerra-csjg.

ZENON SAAVEDRA received the Dr. Eng. degree in electronic engineering and the Ph.D. degree in science and engineering from the National University of Tucuman, Tucuman, Argentina, in 2014 and 2020, respectively.

He is currently a Postdoctoral Research Fellow with the Consejo Nacional de Investigaciones Científicas y Tecnológicas (CONICET), Argentina. His main research interests include signal processing and modelling of radar system.

ADRIAN LLANES received the Eng. degree in electronica engineering from the National University of Tucuman, Tucuman, Argentina in 2018. He is currently working toward the Ph. D. degree in science and engineering from National University of Tucuman, supported by a two-year scholarship in collaboration with the Air Force, Argentina. His main research interests include software development and artificial intelligence.

GONZALO ALDERETE HERO received his degree in electronic engineering with mention in telecommunications at the university of Tucuman in 2021. His thesis was oriented to the calculation and analysis of the Radar Cross Section of maritime and aerial vehicles by means of electromagnetic simulation software. He is currently dedicated to the design and development of electronic circuits for communication systems.

JULIAN DI VENANZIO received the B.S. in aeronautical and aerospace Systems from the Aeronautical University Institute, Cordoba, Argentina in 2002. He received the specialist in radiation protection and safety of radiation sources from the Faculty of

Engineering, University of Buenos Aires, Buenos Aires, Argentina in 2011. Since 2015, he has held various positions in the Dirección General de Investigación y Desarrollo de la Fuerza Aérea Argentina, Argentina. Since 2017, he has been an advisor to the Ministry of Defence of Argentina, Argentina. His main research interests include radar systems and space operations.

ANA G. ELIAS received her PhD in Physics from the National University of Tucuman, Argentina, in 1999. She works there as a CONICET Researcher (Consejo Nacional de Investigaciones Cientificas y Tecnicas) and as a Professor of Statistical Physics. Research interests have included: variability of the upper and lower atmosphere, solar and geomagnetic activity, geomagnetism. Her research now is mainly focused in Sun-Earth interaction, Earth's magnetic field secular variations and reversal scenarios, Ionosphere long-term trends and its connection to Earth's magnetic field and increasing greenhouse gases concentration, and radiowave propagation.

Performance Analysis of a Sky-Wave Over-the-Horizon Radar Simulation Tools

ZENON SAAVEDRA

Facultad de Ciencias Exactas y Tecnología, Universidad Nacional de Tucumán, Tucumán, Argentina

Consejo Nacional de Investigaciones Científicas y Técnicas, Tucumán, Argentina.

ADRIAN LLANES

Facultad de Ciencias Exactas y Tecnología, Universidad Nacional de Tucumán, Tucumán, Argentina

GONZALO ALDERETE HERO

Facultad de Ciencias Exactas y Tecnología, Universidad Nacional de Tucumán, Tucumán, Argentina

JULIAN DI VENANZIO

Dirección Nacional de Investigación y Desarrollo, Fuerza Aérea Argentina, Buenos Aires, Argentina

ANA GEORGINA ELIAS

Facultad de Ciencias Exactas y Tecnología, Universidad Nacional de Tucumán, Tucumán, Argentina

Consejo Nacional de Investigaciones Científicas y Técnicas, Tucumán, Argentina.

***Abstract*— This paper presents the main features of a skywave over-the-horizon radar simulation software and its ability to represent and detect different search scenarios. Through a series of simulations of the primary phenomena involved in the search process, the software can estimate the behaviour of a radar system in various scenarios. This capability allows the simulator to assist in selecting the most suitable radar configuration to achieve an acceptable level of successful detection probability for a given set of scenarios. It also facilitates various studies and analyses of different factors present in the behaviour of these types of radars.**

***Keyword*— OTH Radar, Radar Simulator, Radar System, Signal Processing Radar**

I. INTRODUCTION

Skywave Over-The-Horizon (OTH) radars are specialized radar systems capable of detecting targets beyond the line of sight by leveraging the Earth's ionosphere as a reflector for the radar's emitted electromagnetic waves [1], as is schematically shown in Fig. 1.

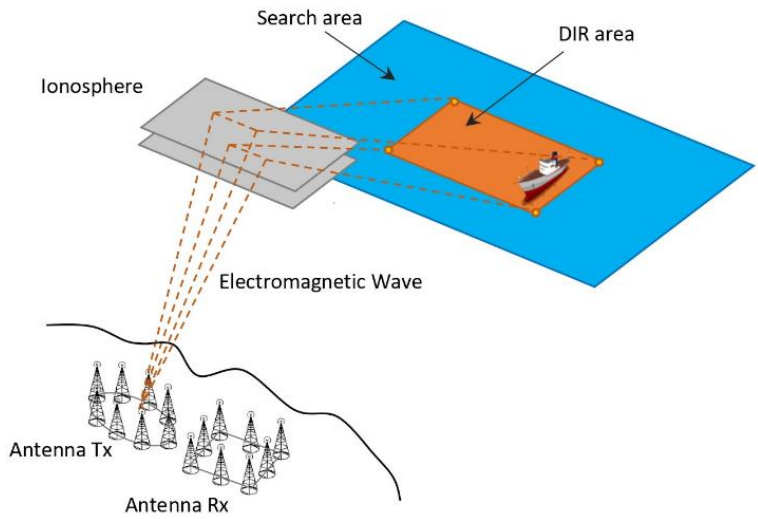

Fig. 1. OTH-SW Radar operates by reflecting its beam from the ionosphere.

The complexity and ionosphere usage of these radars imply a high manufacturing cost and a large number of components, making their preliminary study and design crucial steps before development and deployment. Computer-aided simulations serve

Manuscript received XXXXX 00, 0000; revised XXXXX 00, 0000; accepted XXXXX 00, 0000. This work was supported by the Argentinian Ministry of Defence (PIDDEF program) under Grant 03/2020 and by a Post Doctoral scholarship from CONICET (Argentina) (Corresponding Z. Saavedra.)
Z. Saavedra, A. Llanes, G. Alderete Hero and A. G. Elias are with Universidad Nacional de Tucumán, Tucumán, 4000, Argentina, and also with the Consejo Nacional de Investigaciones Científicas y Técnicas, Tucumán, Argentina (e-mail: zsaavedra@herrera.unt.edu.ar; allanes@herrera.unt.edu.ar; herogonzalo@gmail.com; aelias@herrera.unt.edu.ar).
J. Di Venazio is with the Fuerza Aerea Argentina, Buenos Aires, 1000, Argentina, (e-mail: jdvfaa1@gmail.com).

as an effective methodology for this purpose, enabling designers to define specific radar system configurations and evaluate their performance against various proposed search scenarios. This process would ultimately determine the viability of the chosen configuration.

Several studies have presented partial models of an OTH simulator, including those by Feng et al. (2022) [2], Sun et al. (2022) [3], Cervera et al. (2018) [4] and Zhu et al. (2014) [5]. These works focus on different aspects of the OTH radar system, such as target tracking, wave propagation, interaction with the environment and target, and sea state characterization. However, they leave out other vital aspects for system evaluation, such as signal generation, digital processing, coordinate conversion, and antenna arrays.

In this paper, we propose a comprehensive simulation software that encompasses all these phenomena, providing a more holistic representation for a thorough evaluation and analysis of system performance. Our tool encapsulates the entire search process chain, from the emission of the electromagnetic wave to the visualization of the detections. The software is intended to be included in a process to iteratively adjust the configuration setup, evaluating the alignment of detections with the proposed scenario (see Fig. 2). This leads to more accurate and complete assessment of the system's viability.

This approach gives control to the user to choose which set of parameters to keep constant and which to change. For example, the user can choose to keep the constructive parameters of the radar unchanged and optimize exploration setup for different scenarios. As another example, the user can choose specific scenarios to

detect, and optimize for radar and exploration parameters. If output detections poorly match the proposed ones over different exploration setups, then radar configuration is considered inviable. Otherwise, radar config is considered viable after having acceptable detections over a large enough pool of proposed scenarios.

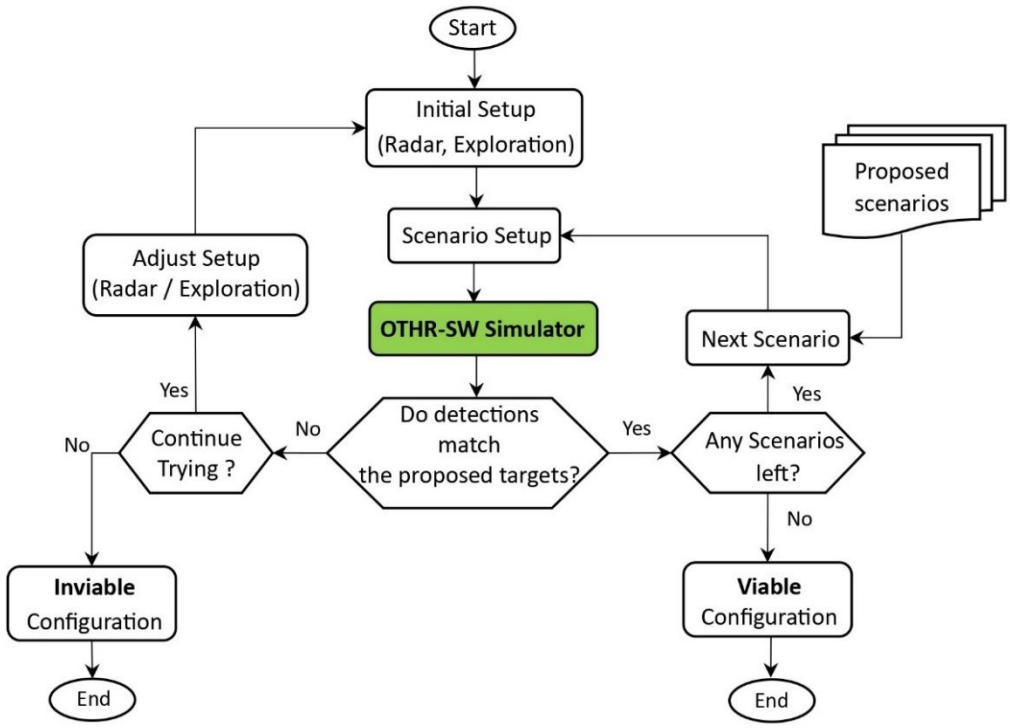

Fig. 2. Evaluation process of a radar configuration against a search scenario.

The rest of paper is organized as follows: in Section 2 we are describing the theoretical models adopted for the OTHR-SW Simulator. The results of simulations and their analyses are presented in Section 3. Conclusions are drawn in Section 4, followed by an appendix which gives further details of the simulator's configurable parameters.

II. METHODOLOGY

The OTH-SW simulator simulates the signal interaction with (i) the medium as it propagates from the transmitting array to the searching area, (ii) the searching area composed of targets and sea, as proposed by the user and (iii) the medium as the reflected energy propagates from the searching area to the receiving array.

After generating the received signal in digital domain, a digital processing module performs the "operative" stage of the radar. Here, a series of filters are applied that progressively de-noise the signal for range, doppler frequency and amplitude estimation. At the final stage, these parameters are converted to geographical coordinates and velocity, respectively. All the simulations process is represented in a block diagram in Fig. 3.

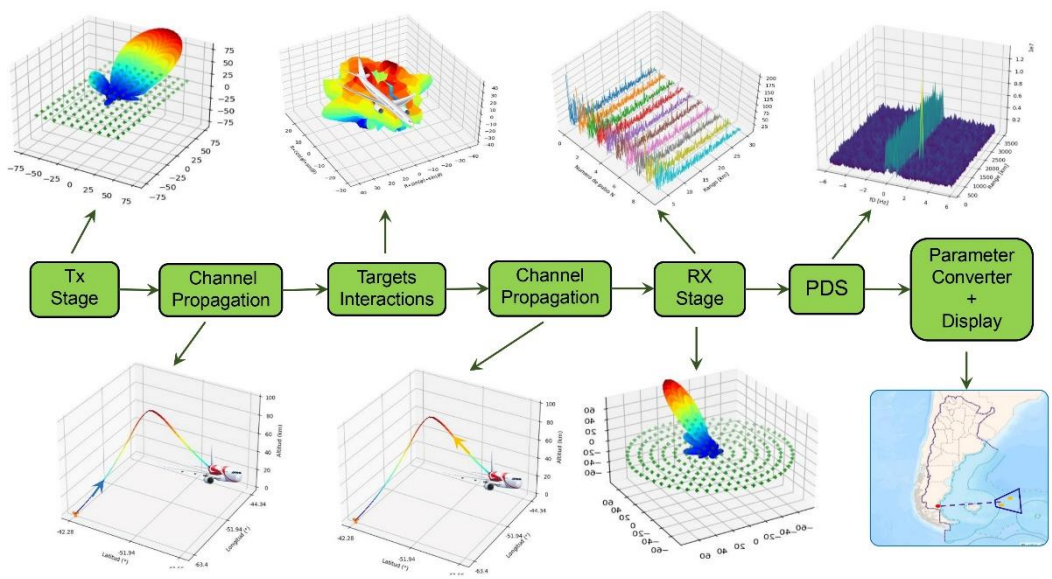

Fig. 3. General block diagram of the Skywave Over-the-Horizon (OTH-SW) Radar Simulation software.

To achieve this, we propose the following implementation scheme (also shown in Fig. 4):

- User Interface: is responsible for the interaction between the user and the simulator tool. It allows the user to input configuration parameters and visualize the output results.
- Core Entrypoint: establishes the communication channel between the front end and the core, synchronizing and controlling the data flow between blocks.
- Core: is the calculation engine of the tool that simulates the signal propagation and the radar operation to recover that signal (see Fig. 3).

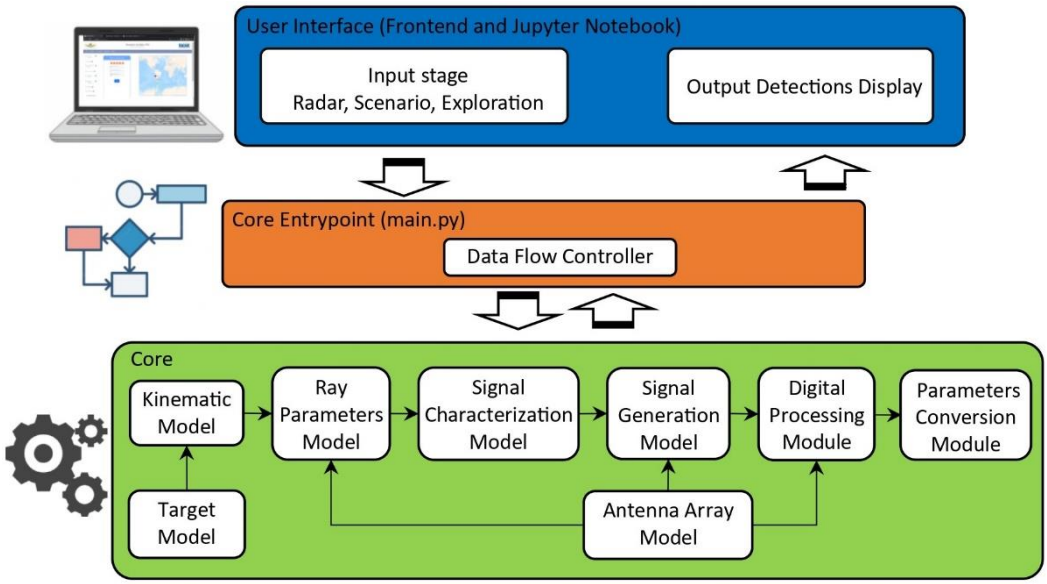

Fig. 4. Implementation scheme of (OTH-SW) Radar Simulation software.

The major blocks in the Fig. 4 are describe below with put focus in the Core implementation.

A. Input stage (Frontend)

The first step of the process is to setup all input configuration parameters exposed to the user. We classified them into a two-tier hierarchy: the top-most level has three groups:

(i) radar setup: constructive parameters of the radar.

(ii) proposed scenario setup: searching area location and targets setup.

(iii) exploration setup: parameters for shaping the exploration signal characteristics.

Each group has subgroups as shown in Fig. 5. A more thorough description can be found in the Appendix.

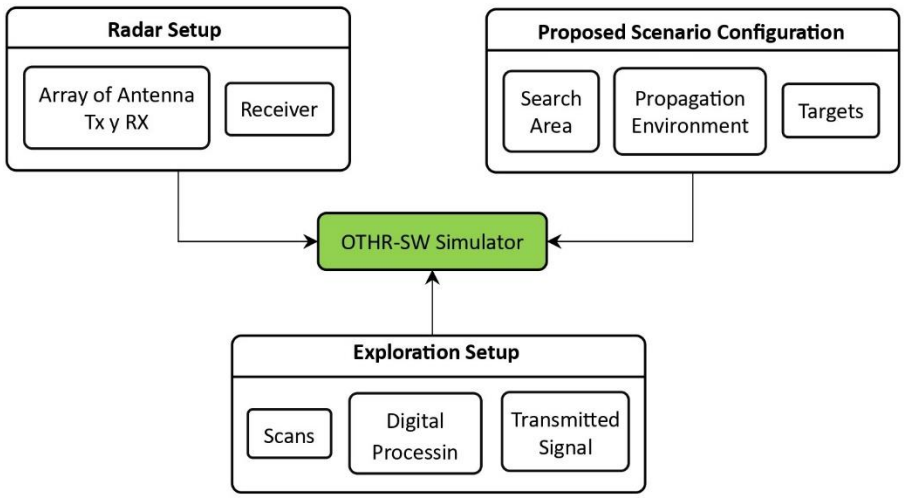

Fig. 5. Possible configuration parameters of the Over-the-Horizon Radar Simulator (OTHR-SW). The parameters are sorted into three groups: radar setup, proposed scenario, and exploration setup.

B. Target Model

The user can set up the targets for the proposed scenario. These are loaded from pre-generated files that contain target the Radar Cross Section (RCS) data.

For this work, RCS data for the following targets has been generated (shown in Fig. 6):

- Boeing 787 Aircraft
- F-117 Aircraft
- Panamax-like Vessel
- Fishing Vessel

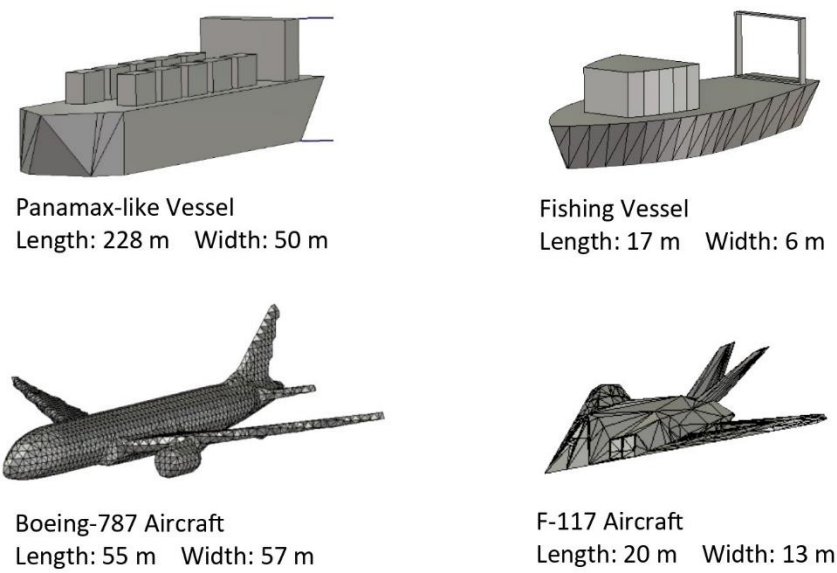

Fig. 6. Types of targets selectable in the Over-the-Horizon Radar Simulator (OTHR-SW).

1) Radar Cross Section

The radar cross section is the ability of an object to reflect a certain percentage of the electromagnetic waves that impact it. Various sources define this factor as a

measure of what "an electromagnetic wave can observe on its propagation path through space". The RCS of a given target depends on aspects such as the physical structure of the target and its external characteristics, the direction of ray incidence, the frequency of the radar transmitter as well as the construction materials of the illuminated object.

In the simulator, the RCS of each target was obtained through an electromagnetic simulator software. The RCS data is stored in matrices as a function of the incident angle, carrier frequency, and wave polarization. Fig. 7 presents a graphical representation of the RCS surfaces of the large plane target.

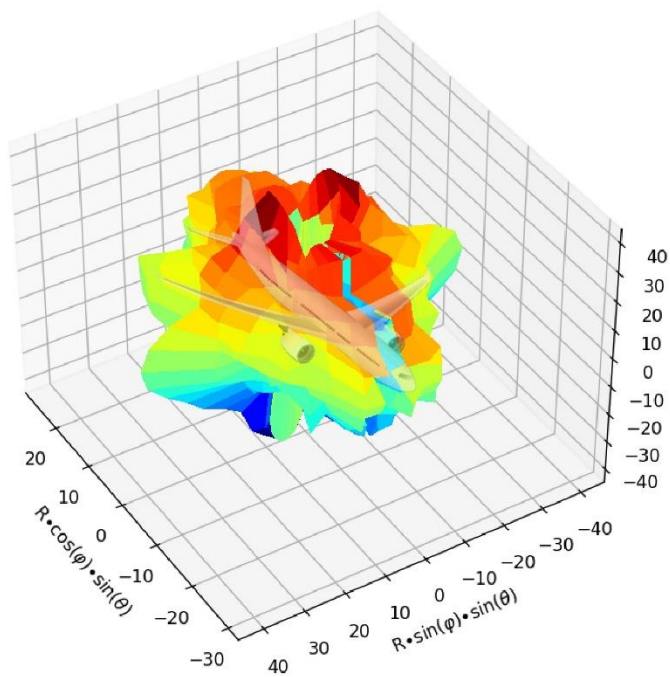

Fig. 7. Diagram of the Radar Cross Section of a large plane type target, at a frequency of 10 MHz, horizontal polarization.

C. Kinematic Array

This model allows evaluating and determining how the position and velocity of the targets evolves over time (see Fig. 8). The possible trajectories they can describe are rectilinear or curvilinear.

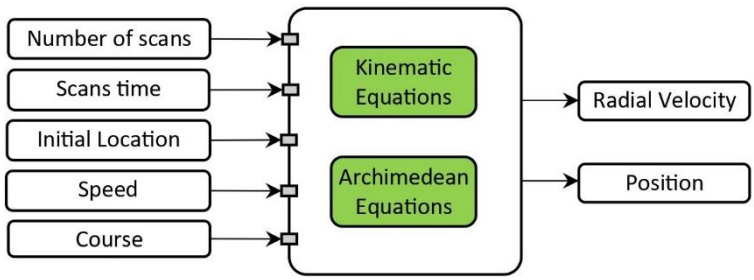

Fig. 8. Kinematic Model of the Targets. Input and output parameters.

An *x*, *y*, *z* coordinate system is used, where the origin matches the location of the radar (See Fig, 9). The variables correspond to latitude, longitude, and altitude, respectively.

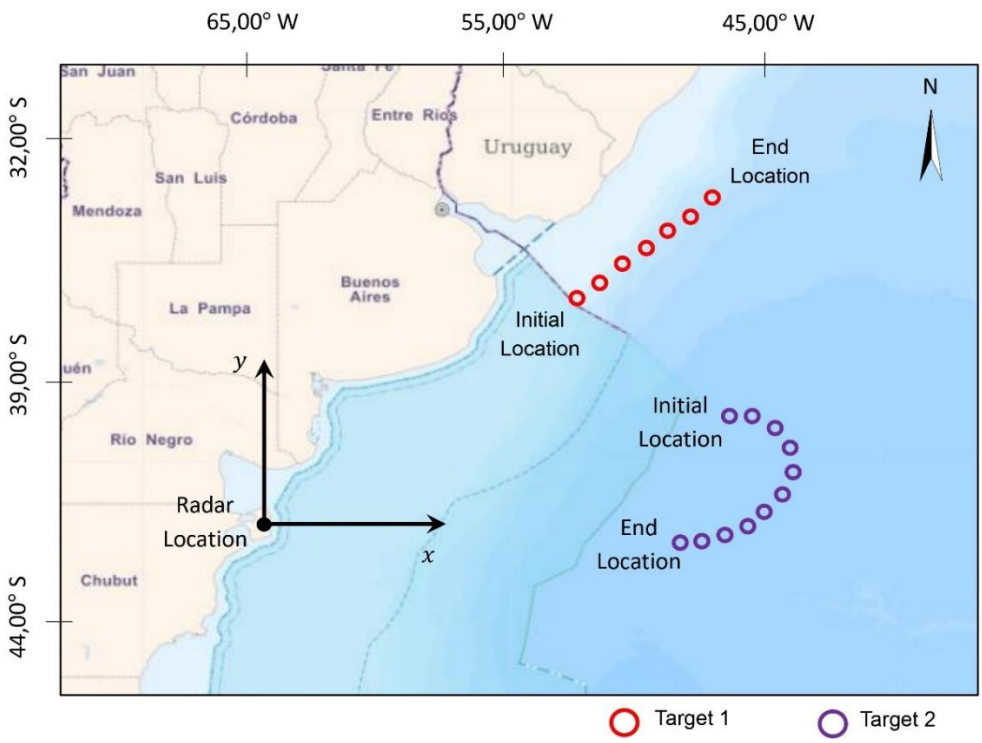

Fig. 9. Representation of the chosen coordinate system, along with an example of the straight and curved trajectories followed by the targets.

For straight trajectories, the determination of the next state of movement in the *x*, *y* plane is based on the equations of classical kinematics for uniform rectilinear motion.

For curved trajectories, the determination of the next state of movement in the *x*-*y* plane is based on the equations of the Archimedean spiral, which in turn is based on polar coordinates.

Finally, the conversion from polar coordinates to rectangular coordinates must be carried out to represent the trajectory in the selected coordinate system. For simplification purposes, the target moves describing the curved trajectory with constant speed.

To determine the positions that the target acquires in its "*z*" axis, which represents the altitude, we used the multipath fading effect based on Earth curvature model [6].

D. Antenna Array Model

This model simulates the behaviour of antennas *arrays*, as the interaction of many individual radiators distributed on a surface that conform either the transmitter or the receiver.

The user can setup the following parameters for each of the arrays: number of elements, geometry type (rectangular, circular, and star), physical separation between elements, radiation pattern of elements (quarter-wave dipole or isotropic radiator) and working frequency.

The array model is presented in Fig. 10.

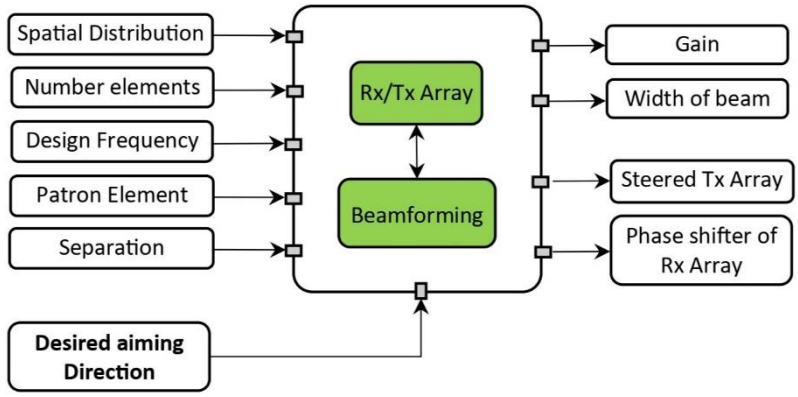

Fig. 10. Transmitter and Receiver antenna array model.

After both the user input and the aiming direction have been defined, the model is able to steer the main lobe of the transmitting array through beamforming techniques. The desired aiming direction is obtained from the Ray Parameters model.

On the other hand, the receiving array simulates the spatial phase shift of the signal received by each element as it propagates through the array. This phase shift information is later used by the Signal Generation model and the Processing Digital Signal model for estimating angle of arrival. Fig. 11 presents three examples of steered transmission arrays.

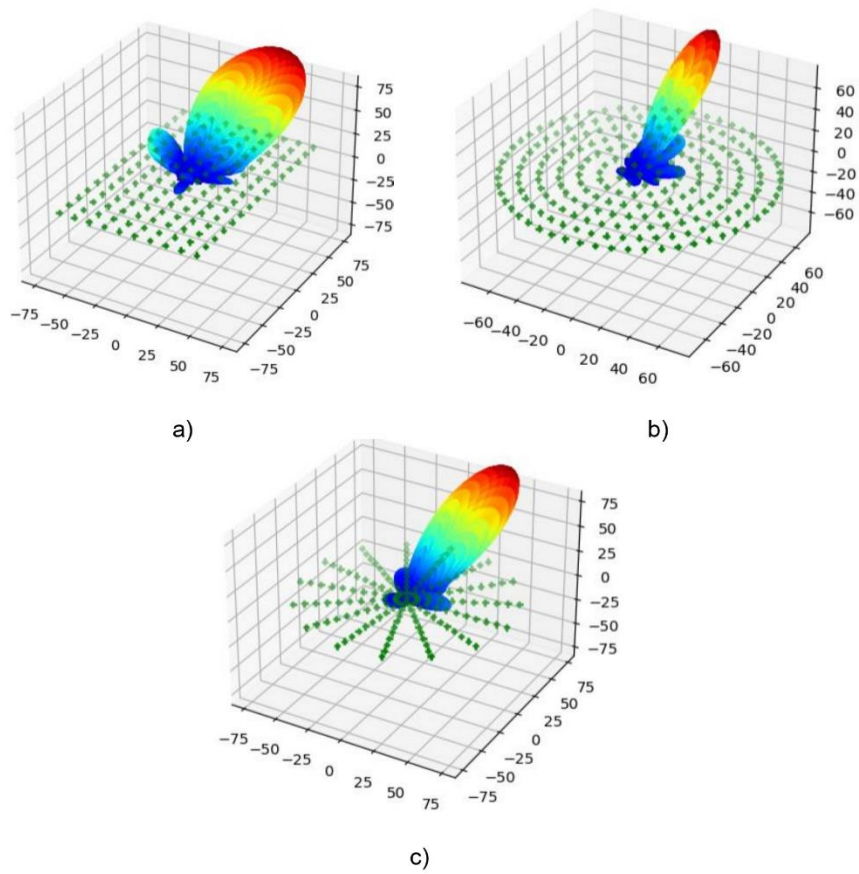

Fig. 11. Transmission arrays with 150 elements with rectangular (a), circular (b), and star distributions (c). Arrays oriented in elevation and azimuth: φ=60 °, θ=20 °.

E. Ray Parameters Model

This model determines the characteristics that an electromagnetic wave must have to achieve propagation in the Earth's ionosphere, between an initial point (radar position) and final point (target position) located on the surface of the Earth or sea. The characteristics of the wave are the frequency, aiming direction, delay, ranges, and propagation attenuation.

The model is composed of two submodels: an analytical ray tracer and an ionosphere modeler, both presented in Fig. 12.

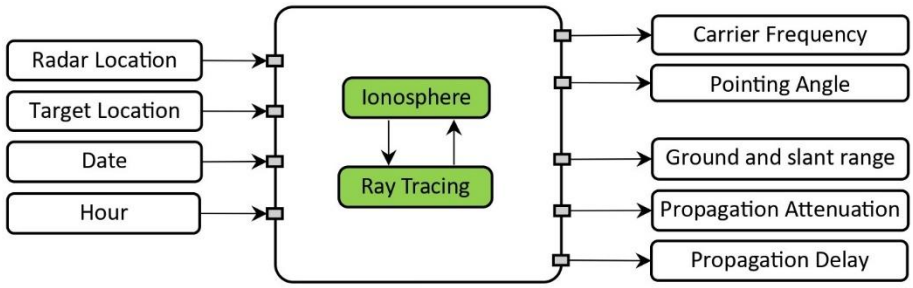

Fig. 12. Ray Parameters Model. Input and output parameters, submodels of Earth's Ionosphere and Ray Tracer.

1) **Ionosphere Model**

The ionosphere model is based on the International Reference Ionosphere model IRI-2012 [7]. The IRI model is the result of the efforts of the scientific community who have worked over the last 60 years to improve and update a standard model of the Earth's ionosphere. This is a complex empirical model that determines different values of the ionosphere state. The most relevant for this study are electron density, critical frequency and peak height of the layers, semi-thickness and composition. These parameters are function of geographic coordinates, date and time; which in turn define the solar activity level on which the ionosphere strongly depends.

2) **Ray Tracing Model**

The ray tracer allows, based on the frequency and direction of an electromagnetic wave, to determine its propagation path within the medium formed by the ionosphere and the lower layers of the troposphere, stratosphere, and mesosphere. An example of the propagation path of a wave determined by the tracer is presented in Fig. 13. The model is based on a system of equations that analytically determine parameters such as: group and phase delay, terrestrial and oblique range reached by the wave [8].

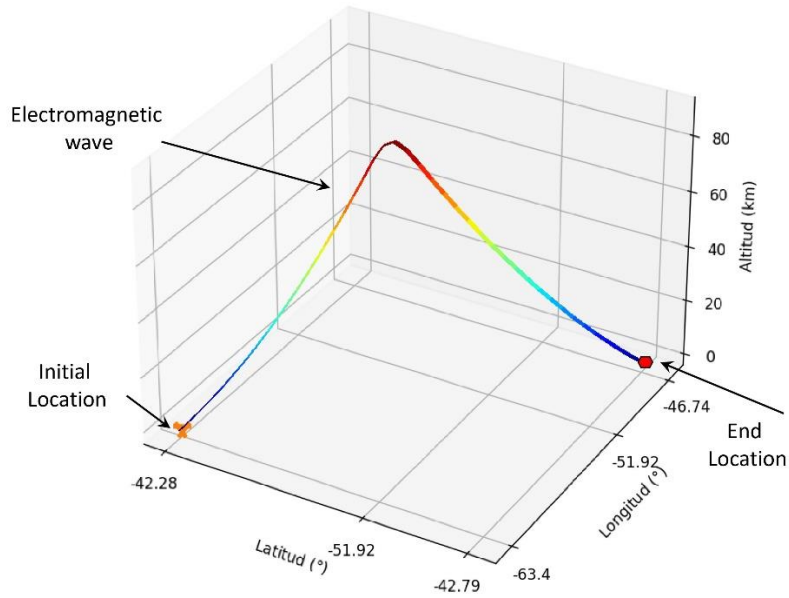

Fig. 13. Example of the path followed by an electromagnetic wave between two points on the Earth's surface.

F. Received Signal Characterization Model

The characterization model determines parameters of the signal received by the receiving system after the electromagnetic wave has interacted with the medium and the proposed scenario. This is important to later generate signals based on the parameters obtained in this stage.

The received signal is modelled according to the following equation.

$$S_R = Echo + Noise + Clutter \quad (1)$$

Where S_R is the received signal, *Echo* is the signal reflected by the targets of interest, *Noise* is an unwanted random signal coming from the surroundings of the antenna arrays and *Clutter* corresponds to the undesired reflection of electromagnetic energy in the surroundings of the targets. For this study, the sea is the Clutter source.

The parameters of interest for the received signal are amplitude levels, frequency, and phase. The mathematical models and equations used in the radio link model can be found in [9][10]. Figure 14 presents a block diagram with the submodels that determine each of the parameters of S_R.

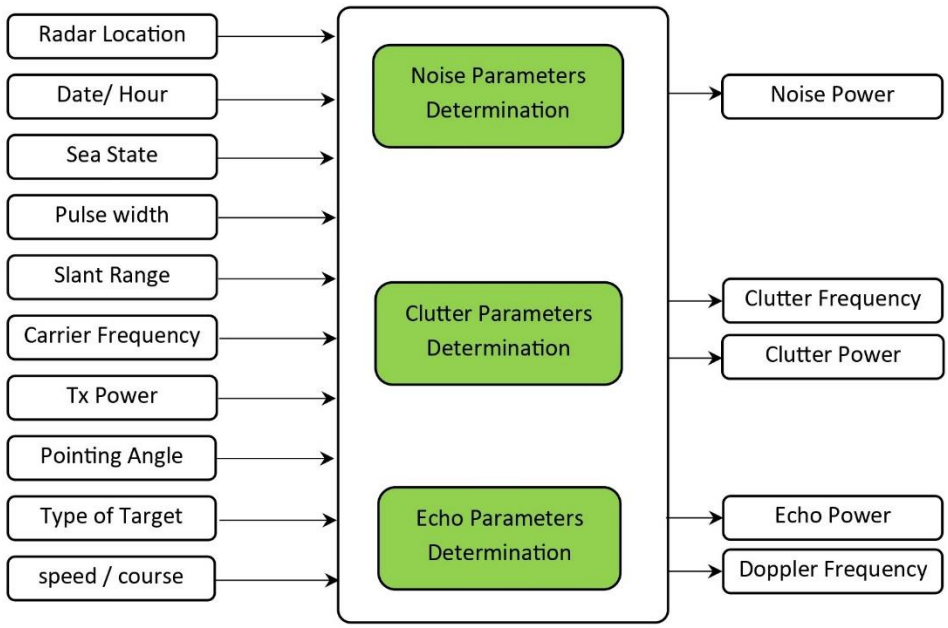

Fig. 14. Model of characterization of the received signal. Input and output parameters, submodels for determining parameters of Noise, Clutter, and Echo.

G. Signal Generation Model

This model is responsible for generating time series of n samples corresponding to the signal received by an antenna array of k elements during a coherent integration interval of m pulses. These are treated as a three-dimensional matrix $\boldsymbol{M}$ $(n \times m \times k)$ for subsequent processing.

Figure 15 shows the block diagram of the signal generator. The simulator is based on a mono-static *pulsed* radar system, where transmission and reception take place at different time intervals.

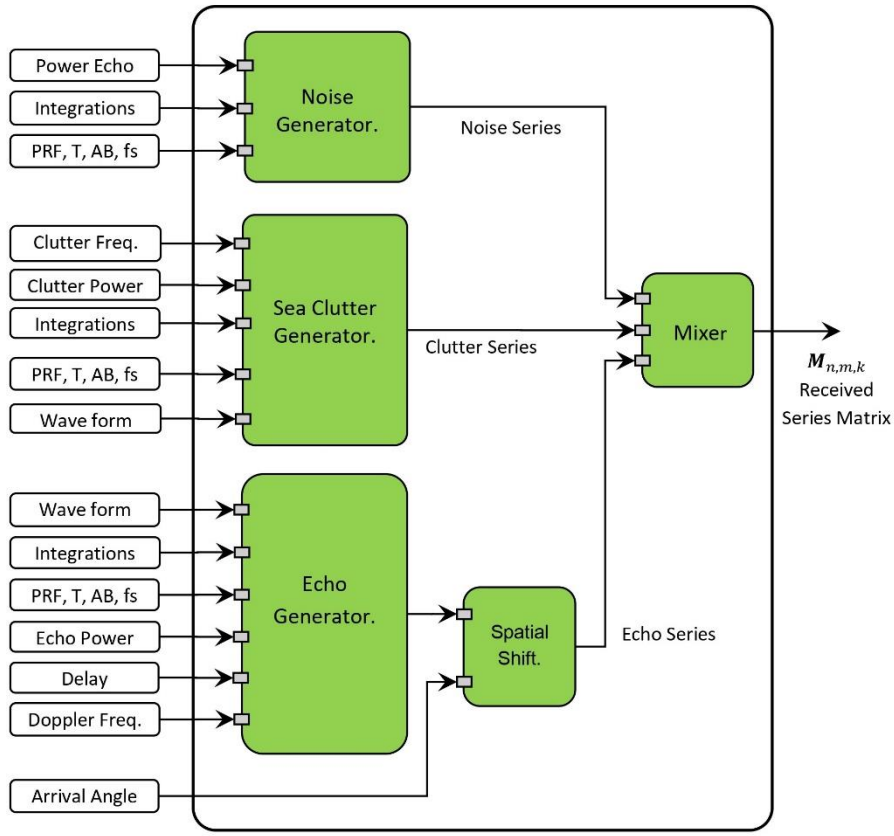

Fig. 15. Received Signal Generation Model. Input and output parameters.

In the model, there are three generators:

- Noise Generator: generates a time series of n samples, based on pulse repetition frequency (PRF) and sampling frequency (f_s). For the amplitude, we use Log-Normal probability distribution function with the average level coming from the Characterization model. The generation of this series is repeated m times, m being the number of integrations.

- Echo Generator: generates a time series of n samples based on *PRF*, pulse width (*T*), bandwidth (*AB*), and sampling frequency. A delay is added to represent the time it takes for the wave to propagate the full round trip (from transmitter to receiver). Additionally, the Doppler Frequency associated with the target's state of motion influences the carrier frequency present in the series. For the amplitude, we use Swerling I-II-III-IV probability distribution function with the average level coming from the Characterization model. The generation of this series is repeated m times, m being the number of integrations.
- Clutter Generator: generates a time series of n samples based on PRF, pulse width, bandwidth, and sampling frequency. For this study we only consider the sea clutter, which is the result of electromagnetic energy impacting the sea surface. This interaction is represented with two spectral lines on each side of 0 Hz. For the amplitude, we use Rayleigh or K probability distribution function with the average level coming from the Characterization model. The generation of this series is repeated m times, m being the number of integrations.

On the other hand, after the Echo series is generated, it enters a Spatial Phase Shifter which models the *reception* of the signal by an antenna array of k elements, where there is a spatial phase shift between the signals received by each antenna element. The phase shift is based on the arrival direction of the signal and the spatial distribution of the receiving antenna array, which can be rectangular, star, and circular.

Finally, the Combiner is responsible for combining the time series of noise, clutter, and echo to obtain the $\boldsymbol{M}$ matrix corresponding to the received signal.

H. Signal Generation Model

This module is responsible for applying various methods and digital data processing techniques to the $\boldsymbol{M}$ matrix of received signal samples, with the aim of extracting range, arrival direction, and Doppler frequency information of potential targets present in the received signals. The block diagram of the processing module is presented in Fig. 16.

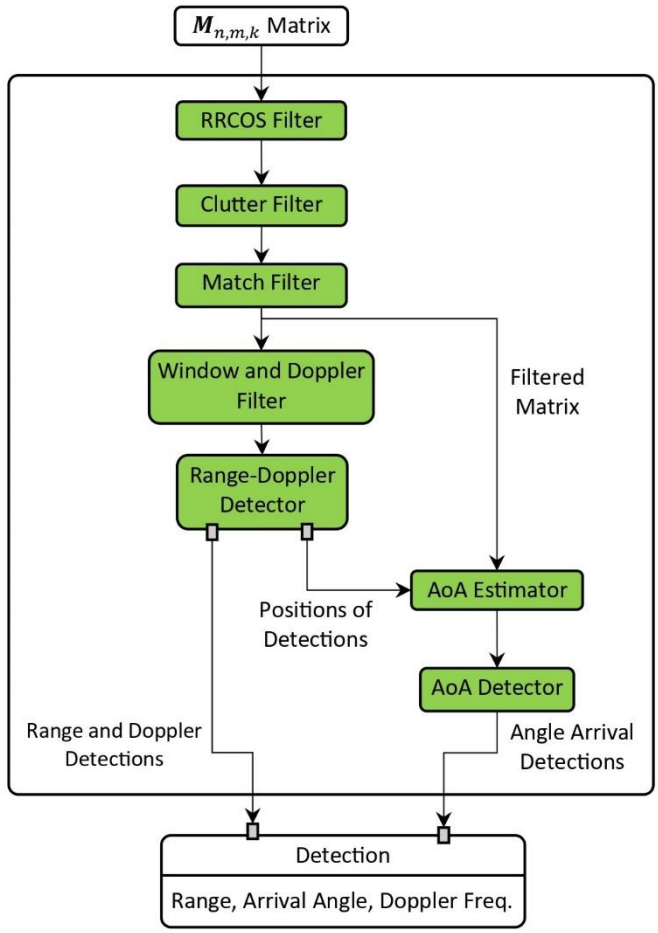

Fig. 16. Digital signal and data processing module.

The tasks performed by each of the blocks are described below.

1) **Raised Root Cosine Filter**

This filter helps reduce the inter-symbol interference produced in the transmission channel. This phenomenon occurs because the signal is modulated with binary codes at the transmitting stage. The filter is applied in the sample domain (along the *n*-axis of the $\boldsymbol{M}$ matrix).

2) **Clutter Filter**

This is responsible for removing the clutter part from the received signal. For this work, the exploration area is always surrounded by the sea. In this case, the energy received is mainly due to the reflections on the sea, as it has greater cross section area than the targets combined, if any [11].

For this purpose, we use the Empirical Mode Decomposition (EMD) technique [12]. This method allows decomposing the signal into its most significant components. We can associate clutter signal to these main components and then filter it out from the received signal. The filter is applied in the sample domain (along the n-axis of the $\boldsymbol{M}$ matrix).

3) **Matched Filter**

This simulator simulates a radar operating under a compressed pulsed mode. This is a very common technique in radar systems to significantly increase SNR figure [13][14]. It relies on (a) encoding the phase of the transmitting signal with some code that optimizes its detection when received, and (b) applying a correlation mechanism on the received signal that detects the presence of the encoded information.

This filter is used for the latter task. It implements the correlation function between the received signal and a copy of the transmitted signal, detecting the *autocorrelation*.

The purpose of this operation is to highlight the delay present between the transmitted signal and the echo signal (signal of interest) present in the received signal. This filter is applied in the sample domain (along the *n*-axis of the ***M*** matrix).

After applying the filter to the ***M*** matrix, the axis (*n*) domain is transformed from samples to range by multiplying each sample by the vacuum speed of light value and dividing by 2, This number is because the determined time considers the round-trip path.

4) **Window and Doppler Filter**

When processing the signal to extract Doppler information (see Doppler Filter) for velocity retrieval, the raw data is segmented into rectangular windows. This introduces significant sidelobes in the frequency domain. To mitigate this problem, the Kaiser-Bessel window is applied before the Doppler filtering. This windowing technique smooths the data and discontinuities at its edges, effectively reducing the sidelobes and resulting in cleaner spectrum for the Doppler filter stage [15]. This filter is applied in the pulse domain (along the *m*-axis of the ***M*** matrix).

On the other hand, the Doppler filter is designed to estimate the relative velocities of detections. When a radar wave bounces off a moving target, the returned signal's frequency changes. The Doppler effect highlights this frequency shift, which is proportional to the object's velocity relative to the radar.

This filter is implemented using Fast Fourier Transform in the pulse domain (along the *m*-axis of the ***M*** matrix). The output is a spectrum where the Doppler frequency components associated with the signal of interest (echo signals) are observed [16].

Finally, we transform the *pulse* axis to *Doppler frequency* axis. The resulting $\boldsymbol{M}$ matrix axis are *range (m)*, *Doppler Frequency (n)* and *number of elements (k)*.

5) **Range-Doppler Detector**

The spectrogram obtained from the Doppler Filter shows how much the received signal is alike the transmitted one. This correlation progressively decays around points of local maxima. An *adaptive detector* is used to detect these points, which are potentially due to the presence of a target.

This stage is implemented using a *Cell Averaging Constant False Alarm Rate* (*CA-CFAR*) detector in two dimensions with a modified refence window: over the *range (m)* and *Doppler Frequency (n)* domains [17].

6) **Angle of Arrival Estimator**

Determines the arrival direction/angle of the received signals with respect to the receiving antenna array. The applied method is called Propagator Direct Data Acquisition (PDDA) [18]. This method is applied in the sample and element domains (along the n and k axes of the $\boldsymbol{M}$ matrix).

The method uses the positions detected (along the range axis) by the Range-Doppler detector as input along with the $\boldsymbol{M}$ matrix filtered by the matched filter. The information from the previously detected positions is used to focus the search on positions where there is already prior knowledge of the possibility of the existence of a potential target echo. After applying this method, the element axis (k) of the $\boldsymbol{M}$ matrix transforms into the angle of arrival axis.

In this point the dimensions of the ***M*** matrix are *n* = range, *m* = Doppler Frequency and *k* = arrival angle.

7) **Angle of Arrival Detector**

After applying the angle of arrival estimator, angle spectrograms (theta and phi) associated with the search area are obtained. The detector allows identifying possible targets within the DIR area and also obtaining phi angle (azimuth) and theta (elevation) values from the spectrograms. The detector is of the adaptive type, in particular, the CA-CFAR in two dimensions. This data processing technique is applied over the range and arrival angle domains (along the *n* and *k* axes of the ***M*** matrix).

Finally, after applying the entire processing chain, a set of detections characterized by range, arrival direction, and Doppler frequency values are obtained, which are suspected to belong to the echoes of targets present in the search area.

I. Radar-to-Geographic Parameters Conversion Module

This module is responsible for transforming the values of range, arrival angle, and Doppler frequency into geographical position and radial speed of the detections (see Fig. 17).

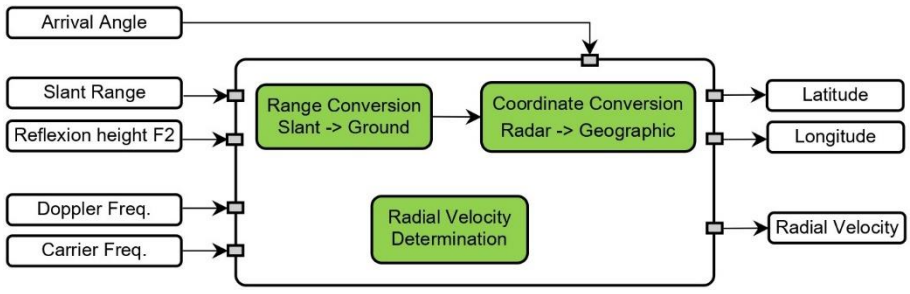

Fig. 17. Radar-to-Geographic Parameter conversion module. Input and output parameters.

The Range Conversion module uses a set of equations to convert the oblique range, which is the propagation path followed by the electromagnetic wave in its full round trip, into ground range, which is the projection of the oblique range onto the earth's surface.

The Coordinate Conversion allows the transformation of radar relative coordinates (ground range and direction) into geographical coordinates (latitude and longitude).

On the other hand, radial speed is determined by multiplying Doppler frequency by the vacuum speed of light value and dividing by carrier frequency of the transmitted signal.

J. Detection Output

The output detections are saved to both an interactive map and a plain table (*csv* file). This tool specifically saves the following files after each exploration:

- ***params.json***: all the parameters setup by the user for this run.
- ***datos_cinematica.csv***: position and speed information for every target set up in the proposed scenario.
- ***mapa_con_detecciones.html***: interactive geographic map for viewing proposed scenario and output detections (see Fig. 18).
- ***resultados.csv***: plain table of output detections.

Fig. 18. Visualization of the detections found, in the User Interface of the simulator (OTHR-SW).

III. RESULT

In this section, we choose a specific radar configuration and evaluate it against two search scenarios:

- Scenario 1: A single target navigating a curved path, with movements towards and away from the radar and points where the radial velocity is null even while in motion.
- Scenario 2: Features multiple targets each pursuing a distinct linear trajectory, operating independently of one another.

The radar system settings, antenna locations, and the search area remain the same across scenarios. The antenna systems have star geometry, comprises 150 elements, and are located in Chubut, Argentina. The center of the DIR exploration region is

located about 1000 km to the east and extends to approximately 1500 km. This represents roughly half the range of these types of radars [19]. We varied the targets quantity and motion and the exploration configuration.

A. Scenario 1

In this case study, we focus on evaluating the OTH-SW simulation tool for positive, negative, and near-zero radial velocity values.

For this, we designed a scenario where a Cargo Ship, being the only target, follows a curved path at constant speed, as illustrated in Fig. 19. This target is be scanned in this simulation, 15 times at intervals of 16 minutes.

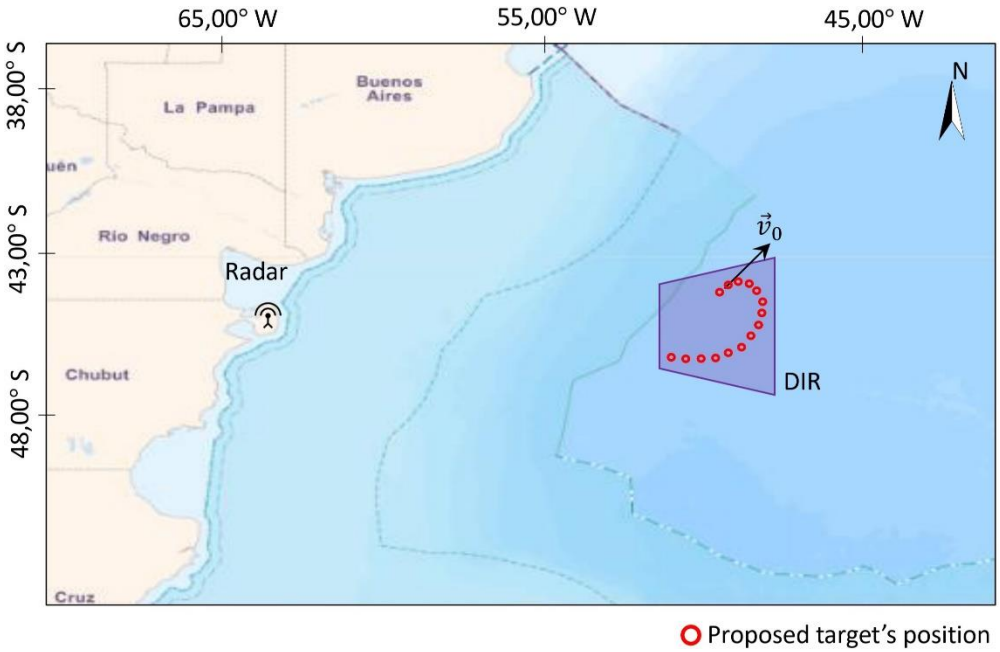

Fig. 19. Representation of the radar system positions, search area, and the target's trajectory.

Tables 1, 2, and 3 detail the parameters configured for: proposed scenario, exploration, and radar system.

TABLE I

Configuration of proposed scenario.

Proposed Scenario Setting	
Search Area	**Value**
Radar Location	42.55 ° S 63.83 ° W
DIR Location	42.70 ° S 51.46 ° W
Target	**Value**
Type	Panama-like
Initial Course	20 º
Initial Speed	11,8 m/s
Path	Curl
Initial Location	42.04° S 51.49° W
Environment	**Value**
Ionosphere State	Calm
Sea State	Moderate (Wave height 1.25 to 2.5 m)
Zone Type	Rural
Date And Hour	2005-05-15T16.00

TABLE II

Configuration of explorations.

Exploration Settings	
Scans	**Value**
Period	16 min
Number of scans	15
Tx Signal	**Value**
Operation mode	Pulsed-Coded
Bandwidth	10 kHz
PRF	40 Hz
Power	40 dBW
Sample Freq.	30 kHz
Code Type	Barker 11
Digital Processing	**Value**
Range-Doppler Detector (Pfa)	$7.0\ 10^{-3}$
Arrival Angle Detector (Pfa)	$4.0\ 10^{-3}$

TABLE III

Configuration of radar.

Radar System Settings	
Antenna Arrays (Tx and Rx)	**Value**
Geometry	Star
Elements	150
Spacing	0.15 λ
Design Freq.	50 MHz
Base pattern	λ/4 dipole
Receiver	**Value**
Signal Gain	250 dB
SNR	40 dB
SCR	20 dB
Inter. Freq.	0.0 Hz
Bandwidth	30 MHz

After setting all parameters, we proceeded with the simulation. Table 4 shows the target's temporal evolution, produced by the Kinematics module. These are the values the tool should identify at the simulation's end. The estimated and proposed values for *(i)* geographic position and *(ii)* radial velocity are shown in Figures 20 and 21, respectively.

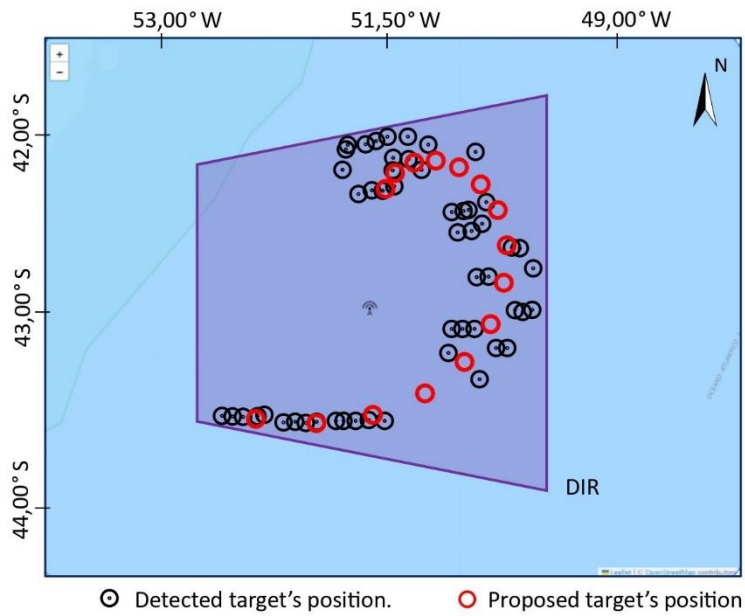

Fig. 20. Detected (in black) and proposed (in red) target positions over the 15 scans.

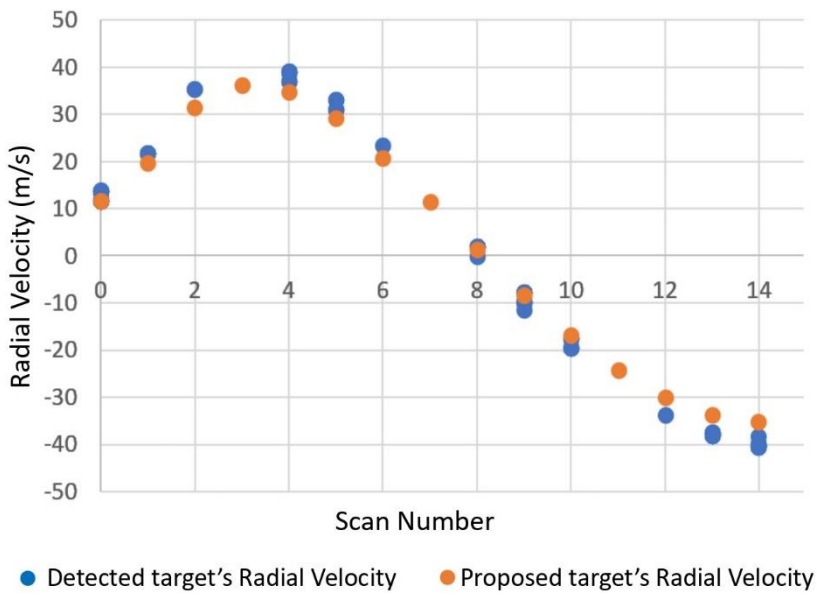

Fig. 21. Detected (in blue) and proposed (in orange) target radial velocity over the 15 scans.

It is important to emphasize that the configuration of the CFAR detector will significantly influence the number of positive detections recorded, due to its

relationship with the false alarm probability. Here we proposed a single target, so we attribute all recorded detections to it. Finally, when calculating the errors, we use the worst of the estimated values for each exploration. The detailed results of this approach can be observed in Table 5, where the errors found in the detections are shown.

TABLE IV

Temporal evolution of the position and radial velocity of the proposed target over the 15 scans.

Proposed Target's Motion		
Scan Nº	**Geographical Location (Lat, Lon)**	**Radial Velocity**
0	42.04° S, 51.49° W	11.8 m/s
1	41.94° S, 51.41° W	19.8 m/s
2	41.89° S, 51.27° W	31.3 m/s
3	41.87° S, 51.10° W	36.2 m/s
4	41.92° S, 50.92° W	34.8 m/s
5	42.02° S, 50.75° W	29.2 m/s
6	42.17° S, 50.62° W	20.9 m/s
7	42.36° S, 50.55° W	11.3 m/s
8	42.59° S, 50.56° W	1.4 m/s
9	42.82° S, 50.67° W	-8.2 m/s

10	43.04° S, 50.88° W	-16.9 m/s
11	43.22° S, 51.19° W	-24.3 m/s
12	43.35° S, 51.58° W	-30.0 m/s
13	43.40° S, 52.04° W	-33.8 m/s
14	43.36° S, 52.53° W	-35.2 m/s

TABLE V

Maximum absolute and relative errors of position and radial velocity. The errors are calculated between the estimated values from the detections and the proposed target values.

Max. Estimated Error		
Scan Nº	**Absolute error Geographical Location**	**Relative error Radial Velocity**
0	39.77 km	0.17
1	40.91 km	0.10
2	30.44 km	0.13
3	No detections	No detections
4	28.04 km	0.12
5	33.01 km	0.13
6	6.30 km	0.12
7	No detections	No detections

8	36.98 km	0.41
9	50.45 km	0.18
10	39.31 km	0.16
11	61.85 km	No detections
12	18.73 km	0.12
13	55.77 km	0.13
14	44.45 km	0.15

In summary, in this case study, the OTH-SW simulation tool was able to track the target adequately along its trajectory, identifying positive, negative, and near-zero radial velocity values.

B. Scenario 2

In this case study, we explore the interactions of three independent targets, each following a straight trajectory. We focus on the evaluation of *simultaneous* detections of all targets, for positive, negative and near-zero radial velocities.

The proposed scenario includes two fishing vessels and a commercial airplane moving on independent trajectories and being explored 10 times at intervals of 13 minutes. The design is illustrated in Fig. 22.

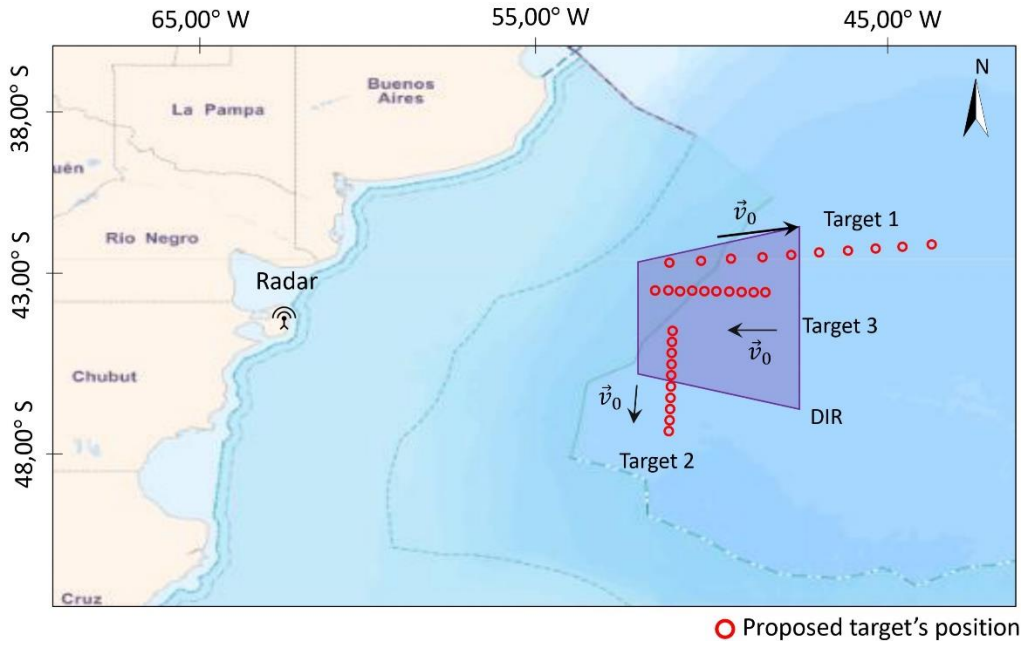

Fig. 22. Representation of the radar system positions, search area, and the trajectory of three targets.

Tables 6, 7, and 8 detail the parameters configured for: proposed scenario, exploration, and radar system.

TABLE VI

Configuration of the proposed scenario.

Proposed Scenario Setting	
Search Area	**Value**
Radar Location	42.55 ° S 63.83 ° W
DIR Location	42.70 ° S 51.46 ° W
Target 1	**Value**

Type	Commercial Aircraft
Initial Course	90 º
Initial Speed	200 m/s
Path	Stright
Initial Location	41.70° S 52.43° W
Target 2	**Value**
Type	Fishing Vessel
Initial Course	180 º
Initial Speed	20 m/s
Path	Stright
Initial Location	43.32° S 52.58° W
Target 3	**Value**
Type	Fishing Vessel
Initial Course	270 º
Initial Speed	40 m/s
Path	Stright
Initial Location	42.68° S 53.09° W
Environment	**Value**
Ionosphere State	Calm
Sea State	Moderate (Wave height 1.25 to 2.5 m)

Zone Type	Rural
Date And Hour	2005-05-15T16.00

TABLE VII

Configuration of exploration.

Exploration Settings	
Scans	**Value**
Period	13 min
Number of scans	10
Tx Signal	**Value**
Operation mode	Pulsed-Coded
Bandwidth	10 kHz
PRF	40 Hz
Power	40 dBW
Sample Freq.	30 kHz
Code Type	Barker 13
Digital Processing	**Value**
Range-Doppler Detector (Pfa)	$1.0\ 10^{-3}$
Arrival Angle	$4.0\ 10^{-4}$

Detector (Pfa)	

TABLE IIX

Configuration of Radar.

Radar System Settings	
Antenna Arrays (Tx and Rx)	**Value**
Geometry	Star
Elements	150
Spacing	0.15 λ
Design Freq.	50 MHz
Base pattern	λ/4 dipole
Receiver	**Value**
Signal Gain	250 dB
SNR	40 dB
SCR	20 dB
Inter. Freq.	0.0 Hz
Bandwidth	30 MHz

After the initialization of the parameters, we executed the simulation. Tables 9a, 10a and 11a show the temporal evolution of each target, determined by the Kinematics

module. These are the values that the tool should recognize at the end of the simulation. Fig. 23 showcase estimated vs. proposed values of geographic position.

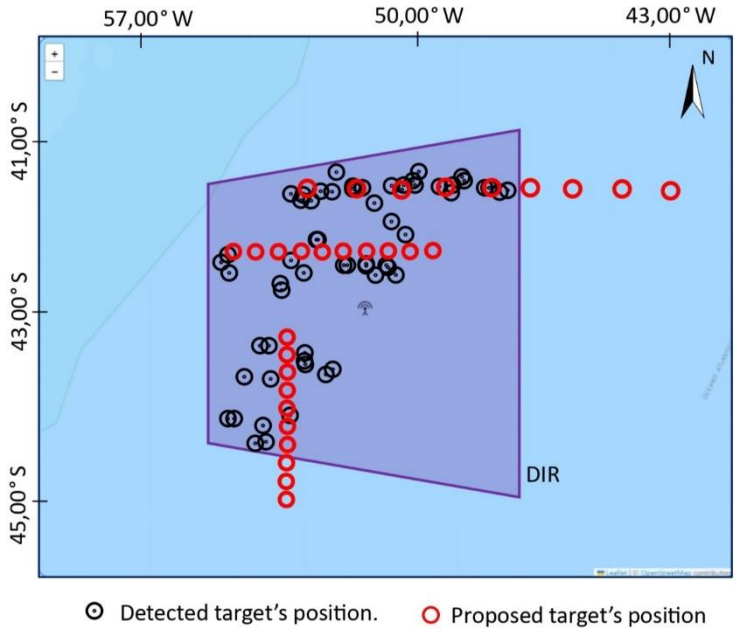

Fig. 23. Detected (in black) and proposed (in red) target positions over the 10 scans.

To address the problem of mapping each detection to each target, we used radial velocity as the main grouping criterion, a strategy illustrated in Fig. 24. Then, in Fig. 25, we compare the proposed radial velocities with those derived from the detections.

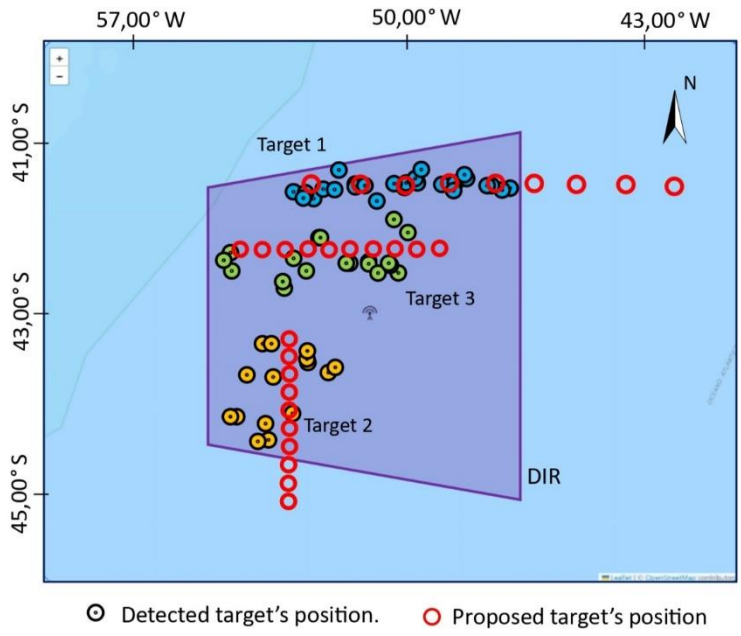

Fig. 24. Detected (in black) and proposed (in red) positions of the three targets over the 10 scans.

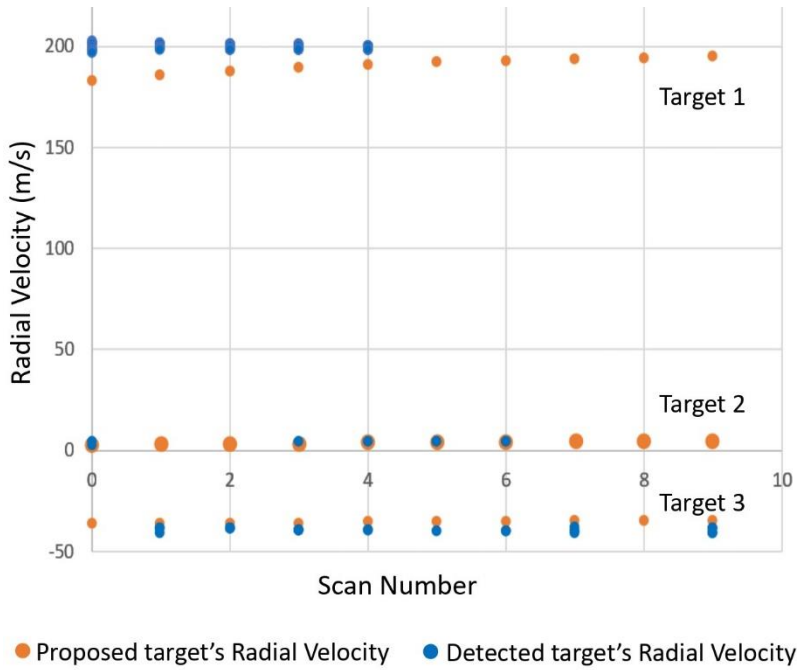

Fig. 25. Detected (in black) and proposed (in red) radial velocity of the three targets over the 10 scans.

Similar to Scenario 1, we took the largest difference found in each exploration to determine the errors in latitude, longitude, and velocity. The most significant errors are detailed in Tables 9b, 10b, and 11b.

In summary, this case study demonstrated that the OTH-SW simulation tool can successfully identifies and follows each target along its respective trajectory, accurately discerning the variations in radial velocities and geographic locations, considering the maximum errors. Thus, this scenario corroborates the tool's ability to handle complex scenarios with multiple targets moving on independent straight trajectories.

TABLE IX

(a) Temporal evolution for Target 1 (Commercial airplane) from Kinematics module. (b) Absolute and relative maximum error for each scan.

Target 1	**Proposed Target's Motion**		**Max. Estimated Error**	
Scan Nº	**Geographical Location (Lat, Lon)**	**Radial Velocity**	**Absolute error Geographical Location**	**Relative error Radial Velocity**
0	41.70 ° S, 52.43 ° W	182.88 m/s	53.98 km	0.106
1	41.70 ° S, 51.35 ° W	185.69 m/s	34.50 km	0.087
2	41.70 ° S, 50.28 ° W	187.74 m/s	37.54 km	0.071
3	41.70 ° S, 49.20 ° W	189.50 m/s	37.48 km	0.060
4	41.70 ° S, 48.12 ° W	190.89 m/s	92.64 km	0.049

5	41.70 ° S, 47.04 ° W	191.96 m/s	No detections	No detections
6	41.70 ° S, 45.96 ° W	192.93 m/s	No detections	No detections
7	41.70 ° S, 44.89 ° W	193.58 m/s	No detections	No detections
8	41.70 ° S, 43.81 ° W	194.17 m/s	No detections	No detections
9	41.70 ° S, 42.73 ° W	194.62 m/s	No detections	No detections

TABLE X

(a) Temporal evolution for Target 2 (Fishing Vessel) from Kinematics module. (b) Absolute and relative maximum error for each scan.

Target 2	**Proposed Target's Motion**		**Max. Estimated Error**	
Scan N°	**Geographical Location (Lat, Lon)**	**Radial Velocity**	**Absolute error Geographical Location**	**Relative error Radial Velocity**
0	43.32 ° S, 52,58 ° W	2.79 m/s	132.26 km	0.445
1	43.43 ° S, 52,58 ° W	3.02 m/s	49.36 km	0.327
2	43.53 ° S, 52,58 ° W	3.24 m/s	No detections	No detections
3	43.64 ° S, 52,58 ° W	3.46 m/s	28.10 km	0.164
4	43.74 ° S, 52,58 ° W	3.67 m/s	48.97 km	0.111
5	43.84 ° S, 52,58 ° W	3.88 m/s	49.38 km	0.045
6	43.95 ° S, 52,58 ° W	4.10 m/s	127.27 km	0.019
7	44.05 ° S, 52,58 ° W	4.31 m/s	No detections	No detections
8	44.15 ° S, 52,58 ° W	4.53 m/s	No detections	No detections

9	44.26 ° S, 52,58 ° W	4.74 m/s	No detections	No detections

TABLE XI

(a) Temporal evolution for Target 3 (Fishing Vessel) from Kinematics module. (b) Absolute and relative maximum error for each scan.

Target 3	**Proposed Target's Motion**		**Max. Estimated Error**	
Scan N°	**Geographical Location (Lat, Lon)**	**Radial Velocity**	**Absolute error Geographical Location**	**Relative error Radial Velocity**
0	-42.69 ° S, 50.51 ° W	-36.40 m/s	No detections	No detections
1	-42.69 ° S, 50.80 ° W	-36.23 m/s	46.58 km	0.076
2	-42.69 ° S, 51.08 ° W	-36.07 m/s	32.71 km	0.082
3	-42.69 ° S, 51.37 ° W	-35.89 m/s	31.44 km	0.094
4	-42.69 ° S, 51.66 ° W	-35.78 m/s	25.67 km	0.104
5	-42.69 ° S, 51.95 ° W	-35.50 m/s	39.59 km	0.129
6	-42.69 ° S, 52.23 ° W	-35.37 m/s	26.48 km	0.131
7	-42.69 ° S, 52.52 ° W	-35.07 m/s	102.74 km	0.094
8	-42.69 ° S, 52.81 ° W	-34.82 m/s	No detections	No detections
9	-42.69 ° S, 53.10 ° W	-34.59 m/s	29.57 km	0.129

IV. DISCUSSION AND CONCLUSION

Throughout this research, we have developed a simulation tool tailored for the preliminary design and assessment of OTH-SW radar systems. This tool excels by

consolidating, within a single platform, a range of functionalities that were previously fragmented across existing literature. It not only embodies capabilities previously explored but takes a step further, modelling additional phenomena and interactions that allow a broader and more accurate evaluation of various radar configurations.

The scenarios outlined in the results section showcase the simulator's ability to *reproduce* real-world conditions with acceptable fidelity, and *detect* positive, negative and near-zero radial velocities; even when multiple targets are present. This translates into a powerful instrument for the preliminary validation of radar configurations, a crucial step towards the construction of *viable* radar systems. With minimal adaptations, the PDS module then can be used an operative radar.

Looking forward, we identify several promising routes to further expand our tool's capabilities. Two upcoming features we are considering are:

- Machine learning techniques for automatic determination of configuration parameters. This should significantly ease the number of iterations needed to arrive at local optimal results.
- Target segmentation and tracking, to identify any number of simultaneous targets present in an exploration region. This should significantly reduce redundant detections and should also allow the prediction of subsequent positions.

Additionally, we highlight the interest expressed by the Argentine Air Force in incorporating our simulator into their Simulation and War Games Center [20], a meaningful validation of the practical and applied potential of our tool.

In conclusion, we have presented an innovative resource that facilitates not only theoretical evaluation but also practical implementations in the field of OTH-SW radars, fostering a pathway for faster and more accurate developments.

APPENDIX

In this appendix, we detail the configurable parameters available in the OTH-SW simulator, categorized into three distinct groups for ease of understanding and management.

The first group encompasses parameters pertaining to the radar configuration itself, delineating the various settings that representing a *constructed* radar, such as location, geometry and electrical characteristics. **Radar system** parameters and their descriptions are shown in Table A.1.

Following this, the second group delineates the parameters that shape the proposed scenario; including the targets present within the search area as well as the environmental ionosphere and sea conditions that will interfere with the signal. **Proposed scenario** parameters and their descriptions are shown in Table A.2.

The final group of exploration parameters delineates how the tool will configure and handle the signal both before transmitting and after receiving. This encapsulates operational choices such as modulation, pulse repetition frequency, and false alarm rates. **Exploration** parameters and their descriptions are shown in Table A.3.

TABLE A1

Radar system configurable parameters and their descriptions.

Radar System Parameters	
Array Antenna **Tx, RX**	**Description**
Geometrical Distribution	Geometrical distribution of antenna array (rectangular, circular, star)
Number of elements	Number of antennas of array
Element spacing	Inter-element spacing in unit of wavelength.
Design Freq.	Design Frequency of array.
Type antenna	Type of individual antenna (isotropic, quarter wave dipole).
Receiver	**Description**
Signal Gain	Signal power gain.
SNR	Receiver output Signal-to-Noise Rate.
SCR	Receiver output Signal-to-Clutter Rate.
Inter. Freq.	Intermediate frequency of receiver
Bandwidth	Bandwidth of receiver

TABLE A2

Proposed scenario configurable parameters and their descriptions.

Proposed Scenario Parameters	
Search Area	**Description**
Radar Geog. Location	Radar system Geographical Location (Latitude, Longitude)
DIR Geog. Location	Dwell Illumination Region Geographical Location (Latitude, Longitude)
Target	**Description**
Type	Type of target (ships or aircraft)
Initial Course	Initial course of target (geographical azimuth).
Initial Speed	Initial speed of target.
Path	Type of path followed by the target (curve, straight).
Geographical Location	Initial Geographical Location of target (Latitude, Longitude).
Environment	**Value**
Ionosphere	Ionosphere state (With, without

State	disturbances). In this version only "without" is available.
Sea State	Sea state (0 - 9). 0: Calm (glassy) and 9: Phenomenal (Hurricane).
Type zone	Type zone where is located of radar system (city, residential, rural, quiet).
Date and Hour	Date and time of start search target.

TABLE A3

Exploration configurable parameters and their descriptions.

Exploration Parameters	
Scans	**Description**
Period	Time interval between scans.
Number of scans	Number of scans over a DIR area.
Tx Signal	**Description**
Operation Mode	Mode of Operation del radar (Pulsed-modulated, Continuous).
Bandwidth	Bandwidth of the transmitted signal.
PRF	Pulse of Frequency Pulse.

Power	Power average of transmitted signal.
Sample Freq.	Sampling frequency for signal generation.
Carrier Freq.	Carrier frequency of transmitted signal.
Code Type	Code used for modulation.
Pulse width	Width of transmitted pulse.
Digital Processing	**Description**
Pfa Range-Doppler	Probability of false alarm used for Range-Doppler detector.
Pfa Arrival Angle Detector	Probability of false alarm used for Arrival Angle detector.

REFERENCES

[1] G. A. Fabrizio Introduction In *High frequency over-the-horizon radar*, 1st ed., New York, USA, McGraw Hill, 2013, pp. 11- 20.

[2] M. Feng *et al.* Research on a simulation model of a skywave over-the-horizon radar sea echo spectrum *Remote Sens.*, vol.14, no 6, pp. 1461, 2022, doi:10.3390/rs14061461.

[3] W. Sun, M. Ji, W. Huang, Y. Ji and Y. Dai vessel tracking using bistatic compact HFSWR *Remote Sens.*, vol. 12, pp .1266, 2020, doi: 10.3390/rs12081266.

[4] M.A. Cervera, D. B. Francis and G. J. Frazer Climatological model of over-the-horizon radar *Radio Science*, vol. 53, pp. 988–1001, 2018, doi: 10.1029/2018RS006607.

[5] Y. Zhu, Y. Wei and Y. Li First order sea clutter cross section for hf hybrid sky-surface wave radar *Radioengineering*, vol. 23, no.4, pp. 1180-1191, 2014.

[6] C. Hou, Y. Wang, and J. Chen Estimating target heights based on the earth curvature model and micromultipath effect in skywave OTH radar *Journal of Applied Mathematics*, vol. 2014, Article ID 424191, pp. 1-14, 2014, doi: 10.1155/2014/424191.

[7] D. Bilitza *et al.* The international reference ionosphere 2012 - a model of international collaboration *Journal of Space Weather and Space Climate*, vol. 4, pp. 1–12, 2014, doi: 10.1051/swsc/2014004.

[8] T. A. Croft and H. Hoogansian Exact ray calculations in a quasi-parabolic ionosphere with no magnetic field *Radio Science*, vol. 3, no.1, 1968, doi: 10.1002/rds19683169.

[9] Z. Saavedra, D. Zimmerman, M. A. Cabrera and A. G. Elias Sky-wave over-the-horizon radar simulation tool *IET Radar Sonar Navig.*, vol. 14, pp. 1773-1777, 2020, doi: 10.1049/iet-rsn.2020.0158.

[10] Z. Saavedra Modelado del canal de propagación de un radar sobre horizonte Ph.D. thesis, Dept. Electric., Electron. and Compu. Tucumán Nacional Univ., Tucumán, Argentina, 2020, https://www.facet.unt.edu.ar/posgrado/wp-content/uploads/sites/54/2022/11/Tesis_ZSaavedra_2020.pdf.

[11] R. H. Khan Ocean-clutter model for high-frequency radar, *IEEE J. Ocean Eng.*, vol. 16, no. 2, pp. 181–188, 1991, doi: 10.1109/48.84134.

[12] I. Mostafanezhad, O. Boric-Lubecke, V. Lubecke and D. P. Mandic Application of empirical mode decomposition in removing fidgeting interference in doppler radar life signs monitoring devices In *Annu. Int. Conf. IEEE Eng. Med. Bio. Soc.*, Minneapolis, MN, USA, 2009, pp. 340-343, doi: 10.1109/IEMBS.2009.5333206.

[13] N. J. Mohamed Nonsinusoidal radar signal design for stealth targets In *IEEE Transactions on Electromagnetic Compatibility*, vol. 37, no. 2, pp. 268-277, 1995, doi: 10.1109/15.385893.

[14] M. A. Cabrera *et al.* Some considerations for different time-domain signal processing of pulse compression radar *Annals of Geophysics*, vol. 53, pp. 5-6, 2010, doi: 10.4401/ag-4758.

[15] A. V. Oppenheim and R. W. Schafer Filter design Techniques In *Discrete-time signal processing*, 2nd ed., New Jersey, USA, Prentice Hall, 1998, pp. 474 - 485.

[16] K. Don How to create and manipulate radar range–doppler plots Def. Sci. Tech. Org., Australia, Tech. Rep. DSTO-TN-1386, Dec. 2014.

[17] W. Wang, R. Wang, R. Jiang, H. Yang and X Wang Modified reference window for two-dimensional CFAR in radar target detection *The Journal of Engineering*, 2019, doi: 10.1049/joe.2019.0687.

[18] M. A. G. Al-Sadoon *et al.* A New Low Complexity Angle of Arrival Algorithm for 1D and 2D Direction Estimation in MIMO Smart Antenna Systems *Sensors*, vol. 17, 2017, doi: 10.3390/s17112631.

[19] G. A. Fabrizio Introduction In *High frequency over-the-horizon radar*, 1st ed., New York, USA, McGraw Hill, 2013, pp. 39 - 41.

[20] CSJG, Centro de Simulación y Juegos de Guerra *Dirección General de Investigación y Desarrollo de la Fuerza Aérea Argentina*, 2023, Argentina. https://www.argentina.gob.ar/fuerzaaerea/direccion-general-de-investigacion-y-desarrollo/centro-de-simulacion-y-juegos-de-guerra-csjg.

ZENON SAAVEDRA received the Dr.Eng. degree in electronic engineering and the Ph.D. degree in science and engineering from the National University of Tucuman, Tucuman, Argentina, in 2014 and 2020, respectively.

He is currently a Postdoctoral Research Fellow with the Consejo Nacional de Investigaciones Científicas y Tecnológicas (CONICET), Argentina. His main research interests include signal processing and modelling of radar system.

ADRIAN LLANES received the Eng. degree in electronica engineering from the National University of Tucuman, Tucuman, Argentina in 2019.

He is currently working toward the Ph. D. degree in science and engineering from National University of Tucuman, supported by a two-year scholarship in collaboration with the Air Force, Argentina. His main research interests include software development and artificial intelligence.

GONZALO ALDERETE HERO received the Eng. degree in electronic engineering with mention in telecommunications at the National University of Tucuman, Tucuman, Argentina in 2021. His thesis was oriented to the calculation and analysis of the Radar Cross Section of maritime and aerial vehicles by means of electromagnetic simulation software. He is currently dedicated to the design and development of electronic circuits for communication systems.

JULIAN DI VENANZIO received the B.S. in aeronautical and aerospace Systems from the Aeronautical University Institute, Cordoba, Argentina in 2002. He received the specialist in radiation protection and safety of radiation sources from the Faculty of Engineering, University of Buenos Aires, Buenos Aires, Argentina in 2011. Since 2015, he has held various positions in the Dirección General de Investigación y Desarrollo de la Fuerza Aérea Argentina, Argentina. Since 2017, he has been an advisor to the Ministry of Defence of Argentina, Argentina. His main research interests include radar systems and space operations.

ANA G. ELIAS received her Ph.D. in physics from the National University of Tucuman, Argentina, in 1999. She works there as a CONICET Researcher (Consejo Nacional de Investigaciones Cientificas y Tecnicas) and as a Professor of Statistical Physics. Research interests have included: variability of the upper and lower atmosphere, solar and geomagnetic activity, geomagnetism. Her research now is mainly focused in Sun-Earth interaction, Earth's magnetic field secular variations and reversal scenarios,

Ionosphere long-term trends and its connection to Earth's magnetic field and increasing greenhouse gases concentration, and radiowave propagation.